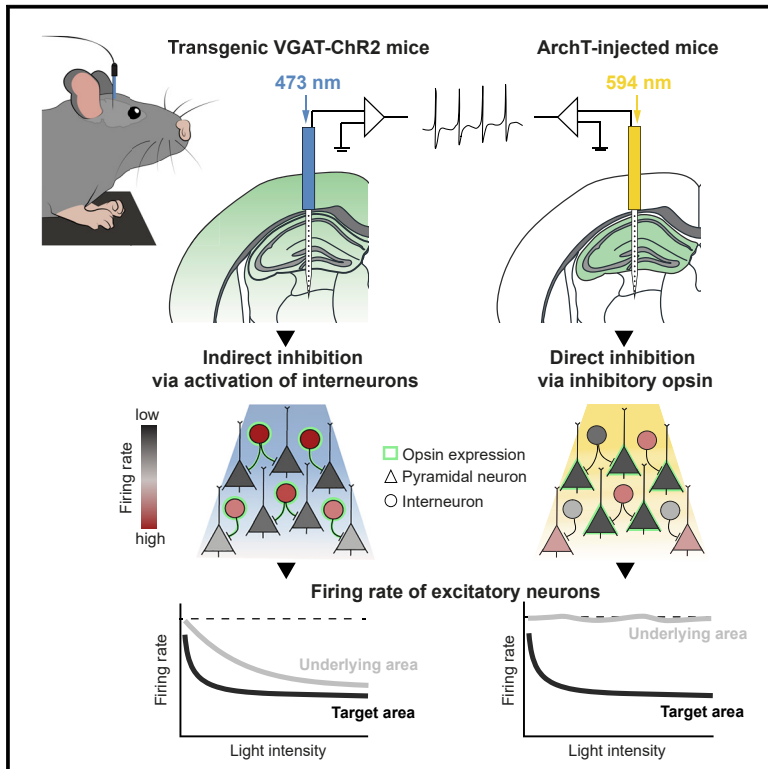


# Cell Reports

## The Spatial Extent of Optogenetic Silencing in Transgenic Mice Expressing Channelrhodopsin in Inhibitory Interneurons

### Graphical Abstract



### Authors

Susanne Stefanie Babl,  
Brian Paul Rummell, Torfi Sigurdsson

### Correspondence

sigurdsson@em.uni-frankfurt.de

### In Brief

Optogenetic silencing is often achieved using transgenic mice expressing channelrhodopsin in GABAergic neurons. Babl et al. demonstrate that this strategy causes spatially extensive inhibition that can extend beyond brain regions targeted for silencing, whereas virally mediated expression of an inhibitory opsin enables regionally restricted inhibition.

### Highlights

- Light delivery in VGAT-ChR2 mice causes spatially extensive inhibition
- Even low light intensities can cause inhibition beyond the targeted brain region
- This effect is consistent throughout various cortical and subcortical regions
- Virus-mediated expression of an inhibitory opsin allows for region-specific silencing



# The Spatial Extent of Optogenetic Silencing in Transgenic Mice Expressing Channelrhodopsin in Inhibitory Interneurons

Susanne Stefanie Babl,<sup>1</sup> Brian Paul Rummell,<sup>1</sup> and Torfi Sigurdsson<sup>1,2,\*</sup><sup>1</sup>Institute of Neurophysiology, Neuroscience Center, Goethe University, Frankfurt, Germany<sup>2</sup>Lead Contact\*Correspondence: [sigurdsson@em.uni-frankfurt.de](mailto:sigurdsson@em.uni-frankfurt.de)<https://doi.org/10.1016/j.celrep.2019.09.049>

## SUMMARY

Optogenetic stimulation of inhibitory interneurons has become a commonly used strategy for silencing neuronal activity. This is typically achieved using transgenic mice expressing excitatory opsins in inhibitory interneurons throughout the brain, raising the question of how spatially extensive the resulting inhibition is. Here, we characterize neuronal silencing in VGAT-ChR2 mice, which express channelrhodopsin-2 in inhibitory interneurons, as a function of light intensity and distance from the light source in several cortical and subcortical regions. We show that light stimulation, even at relatively low intensities, causes inhibition not only in brain regions targeted for silencing but also in their subjacent areas. In contrast, virus-mediated expression of an inhibitory opsin enables robust silencing that is restricted to the region of opsin expression. Our results reveal important constraints on using inhibitory interneuron activation to silence neuronal activity and emphasize the necessity of carefully controlling light stimulation parameters when using this silencing strategy.

## INTRODUCTION

Optogenetic tools have become crucial for manipulating brain areas with high temporal precision in order to decipher their causal role in behavior. Optogenetic silencing is frequently achieved with inhibitory light-sensitive proteins (opsins), which can be expressed in neurons by using viral expression constructs delivered to a brain region of interest (Yizhar et al., 2011). When stimulated with light, inhibitory opsins cause hyperpolarization, enabling rapid and reversible silencing of neuronal activity (Chow et al., 2010; Wiegert et al., 2017; Zhang et al., 2007). Alternatively, neuronal inhibition can be achieved indirectly by optogenetically stimulating gamma-aminobutyric acid (GABA)ergic interneurons. This approach is increasingly being used with the help of transgenic mouse lines expressing the excitatory opsin channelrhodopsin-2 (ChR2) in GABAergic neurons throughout the brain (Asrican et al., 2013; Madisen et al., 2012; Zhao et al., 2011), the most common of which expresses ChR2 under the control of the promoter for the vesic-

ular GABA transporter (VGAT-ChR2 line; Zhao et al., 2011). To date, VGAT-ChR2 mice have been used in a number of studies to inactivate both cortical and subcortical areas during a variety of behavioral tasks (see for example Goard et al., 2016; Guo et al., 2014, 2017; Le Merre et al., 2018; Mathis et al., 2017; Resulaj et al., 2018; Sreenivasan et al., 2016; Wimmer et al., 2015).

When silencing a brain area, it is crucial to avoid directly affecting neighboring structures. If inhibitory opsins are expressed using viral methods, spatial specificity can be achieved by restricting opsin expression to the region of interest. In contrast, in transgenic mice with brain-wide expression of ChR2 in GABAergic neurons (such as the VGAT-ChR2 line), the spatial extent of inhibition is critically dependent on the spread of light that is used to activate ChR2. This, in turn, depends both on the intensity and wavelength of the applied light as well as the light scattering properties of brain tissue (Aravanis et al., 2007; Yizhar et al., 2011), which can vary considerably from one brain region to the next due to differences in tissue microstructure (Al-Juboori et al., 2013; Azimipour et al., 2015). A further complicating factor when using mouse lines such as VGAT-ChR2 is that the spatial extent of inhibition will also depend on the axonal arborizations of the stimulated GABAergic interneurons, which vary substantially depending on interneuron subtype and brain region (Pelkey et al., 2017; Tepper et al., 2018; Tremblay et al., 2016). GABAergic interneurons can also give rise to long-range projections targeting other brain regions (Caputi et al., 2013; Lee et al., 2014; Melzer et al., 2017). These considerations suggest that it is not straightforward to estimate the spatial spread of inhibition caused by optogenetically activating GABAergic interneurons and, thus, the light intensities required for achieving region-specific silencing. A detailed experimental assessment is, therefore, needed.

To address this, we examined the spatial extent of neuronal silencing caused by optogenetically activating GABAergic neurons in VGAT-ChR2 mice and to what extent region-specific silencing is possible by using this approach. To this end, we delivered light to several different cortical and subcortical structures while monitoring neural activity both in these target structures as well as in their subjacent areas. We show that even with relatively low light intensities, neuronal inhibition in VGAT-ChR2 mice can extend to regions that are not intended to be silenced, at least as far as 1.7 mm away from the light source. Our results also demonstrate that robust silencing is observed in areas with weak ChR2 expression and that the spatial profile of inhibition can be complex, possibly reflecting interneuron



arborization patterns. Finally, we show that virally expressing an inhibitory opsin enables optogenetic silencing that is both robust and restricted to the target region. Taken together, our results reveal important constraints on the spatial specificity of neuronal silencing caused by interneuron activation and emphasize the necessity of carefully controlling light stimulation parameters when using this approach.

## RESULTS

### Light Delivered to the Hippocampus in VGAT-ChR2 Mice Causes Neuronal Inhibition Extending to the Subjacent Thalamus

In order to examine the spatial specificity of neuronal inhibition caused by interneuron activation in VGAT-ChR2 mice (Figures 1A and 1B; Figure S1), we first attempted to selectively silence the hippocampus. To this end, we delivered light to the dorsal hippocampus (dHPC) of awake head-fixed VGAT-ChR2 mice while simultaneously monitoring neuronal activity in the dHPC and subjacent thalamus. This was achieved using an “optoprobe,” consisting of a silicon probe attached to an optic fiber, which was inserted into the brain so that the tip of the optic fiber sat above the dHPC (Figure 1C; see STAR Methods). The recording sites of the optoprobe spanned the entire dorsoventral axis of the dHPC and also extended into the underlying lateral posterior (LP) nucleus of the thalamus. The location of the optoprobe was later confirmed using several electrophysiological signatures of the different hippocampal layers (see STAR Methods; Figure S2); sessions were included for analysis where the optic fiber sat just above the pyramidal layer (PL) of the dHPC ( $400.00 \pm 27.39 \mu\text{m}$  above PL;  $n = 16$  recordings from 5 mice). The PL was also used as an anatomical reference point for other brain areas (STAR Methods). Consistent with previous reports *in vitro* (Zhao et al., 2011), application of blue light (473 nm, 1-s duration, 0.5 to 16 mW) caused excitation in some dHPC neurons (Figures 1D and 1F) and inhibition in others (Figure 1E). Both excited and inhibited cells showed a persistent increase or decrease, respectively, in mean firing rates throughout the light pulse duration (Figures S3A and S3D). Excited neurons responded at a short latency to light pulses (Figures S3B and S3C), indicating a direct excitatory effect, and had a narrower waveform than inhibited cells (Figures S4A–S4F). This suggests that excited cells were likely GABAergic interneurons, whereas inhibited cells were most likely excitatory neurons. Across the population of neurons recorded in the dHPC ( $n = 206$  from 5 mice), the percentage of excited and inhibited neurons (see STAR Methods) increased with increasing laser intensity (Figures 1H and 1I).

We next asked whether neuronal silencing was restricted to the hippocampus by analyzing neurons recorded simultaneously in the subjacent LP thalamus ( $n = 46$  from 5 mice). In comparison to the dHPC, the fraction of LP neurons recorded that were excited by light stimulation was relatively low (Figure 1H; 4/46 neurons at 16 mW). Nonetheless, we found that many LP neurons were inhibited by light delivery (Figures 1G and 1I). The lowest light intensity of 0.5 mW was already sufficient to inhibit a significant fraction of neurons (10/46,  $p < 0.0001$ , binomial test), and this fraction increased with increasing light intensity

to approximately 60% (28/46 neurons) at 16 mW (Figure 1I). Histological examination revealed that ChR2-positive neurons were sparse in the LP thalamus (Figure S1D), consistent with the relative lack of excited cells and low numbers of inhibitory neurons reported in this region (Evangelio et al., 2018). However, ChR2-positive axonal terminals were clearly visible (Figure S1D), whose activation could have contributed to the inhibition of LP neurons during light stimulation.

To compare the strength of inhibition in the dHPC and LP, we calculated normalized firing rates during light delivery in the two regions. For this purpose, we excluded neurons that were significantly excited by light stimulation in order to restrict our analysis to putative excitatory neurons (see STAR Methods). In both dHPC and LP, normalized firing rates decreased with increasing light intensity (Figure 1J; main effect of intensity in an area X intensity ANOVA,  $p < 0.00001$ ) and were overall lower in the dHPC than in the LP (main effect of area,  $p < 0.00001$ ). However, inhibition was significant in the LP at all intensities tested (sign-rank test of normalized firing rates,  $p < 0.002$  for all intensities), reaching approximately a 50% reduction in firing rates for intensities of 6 mW or higher (normalized rates at 6 mW,  $0.49 \pm 0.05$ ). Notably, 6 mW was also the intensity at which inhibition strength reached its maximum in the dHPC, which was only slightly higher than in LP (normalized rates,  $0.37 \pm 0.03$ ). At higher intensities, inhibition strength became increasingly more similar in the two regions and did not differ significantly at the highest intensity (Figure 1J; dHPC:  $0.40 \pm 0.05$ ; LP:  $0.37 \pm 0.06$ ;  $p = 0.31$ , rank-sum test). To examine the spatial profile of inhibition in more detail, we quantified neural responses as a function of distance from the optic fiber (Figures 1K–1M). This revealed that inhibition strength gradually decreased with increasing distance but was still significant 1.4–1.7 mm away (Figure 1M; normalized firing rates,  $p < 0.001$  for all intensities), where LP neurons were located. Taken together, these results demonstrate that delivery of light to one target region (the dHPC) in VGAT-ChR2 mice can cause spatially extensive inhibition that also encompasses subjacent structures.

### Light Delivery to the Parietal Cortex in VGAT-ChR2 Mice Causes Neuronal Inhibition Extending to the Subjacent Hippocampus

Although we observed robust inhibition extending to the thalamus when we attempted to silence the hippocampus in VGAT-ChR2 mice, it is unclear whether such widespread inhibition would be observed when targeting other brain regions. VGAT-ChR2 mice have been frequently used to silence cortical areas (see for example Goard et al., 2016; Guo et al., 2014; Sreenivasan et al., 2016), but it is unclear to what extent inhibition can extend to subcortical structures in such experiments. We therefore next asked whether neuronal silencing targeting the cortex in VGAT-ChR2 mice could extend to the hippocampus, which lies immediately below many cortical regions. To this end, we positioned our optoprobe so that the optic fiber sat right above the surface of the posterior parietal association cortex ( $263.89 \pm 17.06 \mu\text{m}$  above surface;  $n = 18$  recordings from 5 mice), allowing us to record simultaneously from the cortex and the subjacent dHPC during light delivery (Figure 2A). As

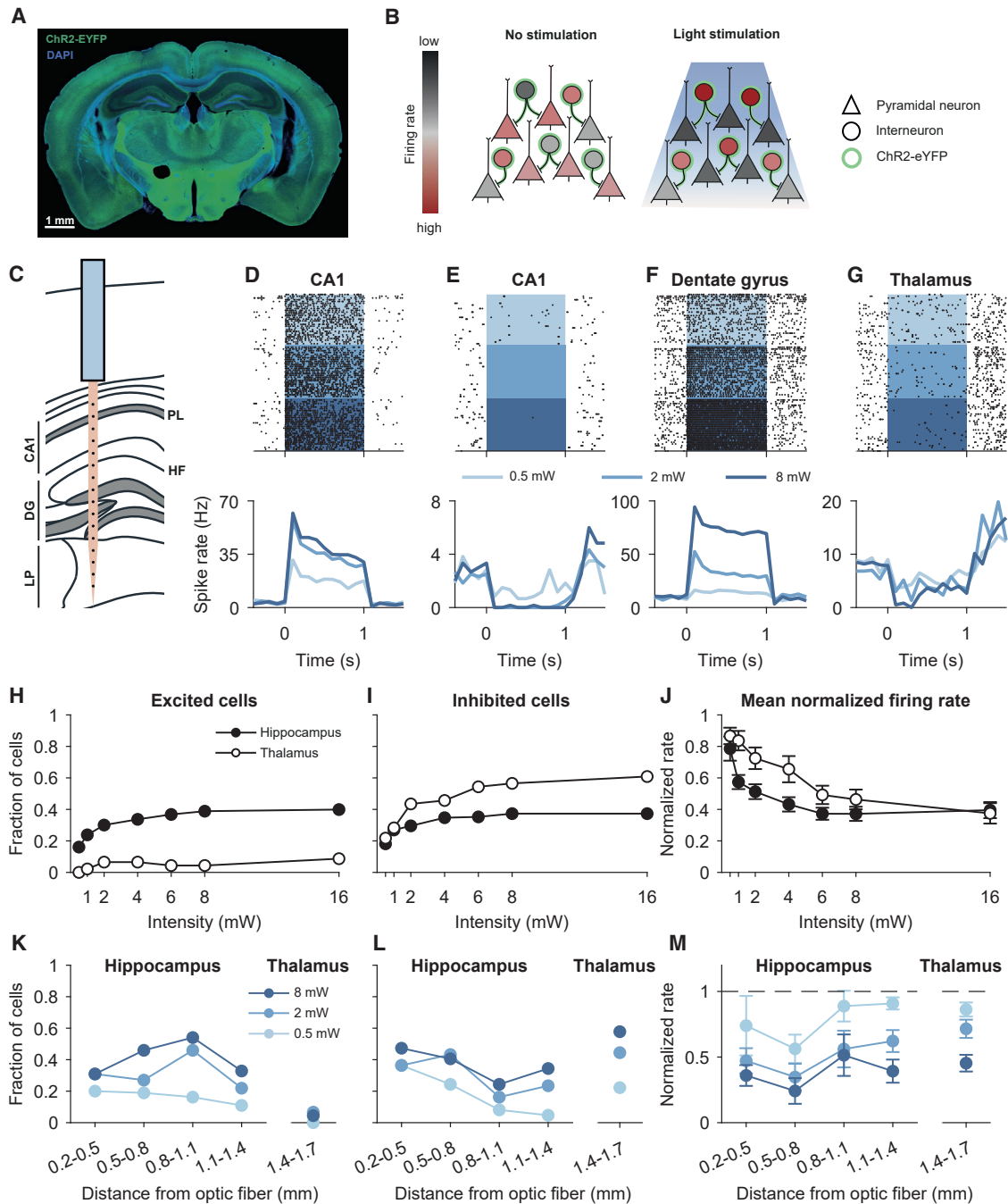


**Figure 1. Light Delivered to the Hippocampus in VGAT-ChR2 Mice Causes Neuronal Inhibition Extending to the Subjacent Thalamus**

(A) Coronal brain section from a VGAT-ChR2 mouse showing expression of ChR2-EYFP.  
 (B) Stimulation of GABAergic neurons in VGAT-ChR2 mice with blue light inhibits the firing of surrounding pyramidal neurons.  
 (C) Schematic of recording configuration; an optoprobe was positioned with the optic fiber above the CA1 pyramidal layer (PL) and recording sites spanning the hippocampus and subjacent LP thalamus. DG, dentate gyrus; HF, hippocampal fissure.  
 (D–G) Raster plots (top) and averaged spike rates (bottom) of example cells recorded in CA1 (D and E), dentate gyrus (F), and thalamus (G) showing excitation (D and F) and inhibition (E and G) to light pulses of different intensities.  
 (H and I) Fraction of significantly excited (H) and inhibited (I) cells in the hippocampus and thalamus at different light intensities.  
 (J) Normalized firing rates of putative excitatory neurons as a function of light intensity. Neuronal inhibition was observed in both structures at all light intensities.  
 (K–M) Fraction of excited (K) and inhibited (L) cells and normalized firing rates (M) as a function of distance from the optic fiber. Firing rates were significantly decreased at a distance of 1.4–1.7 mm. Error bars represent the mean  $\pm$  SEM over neurons.

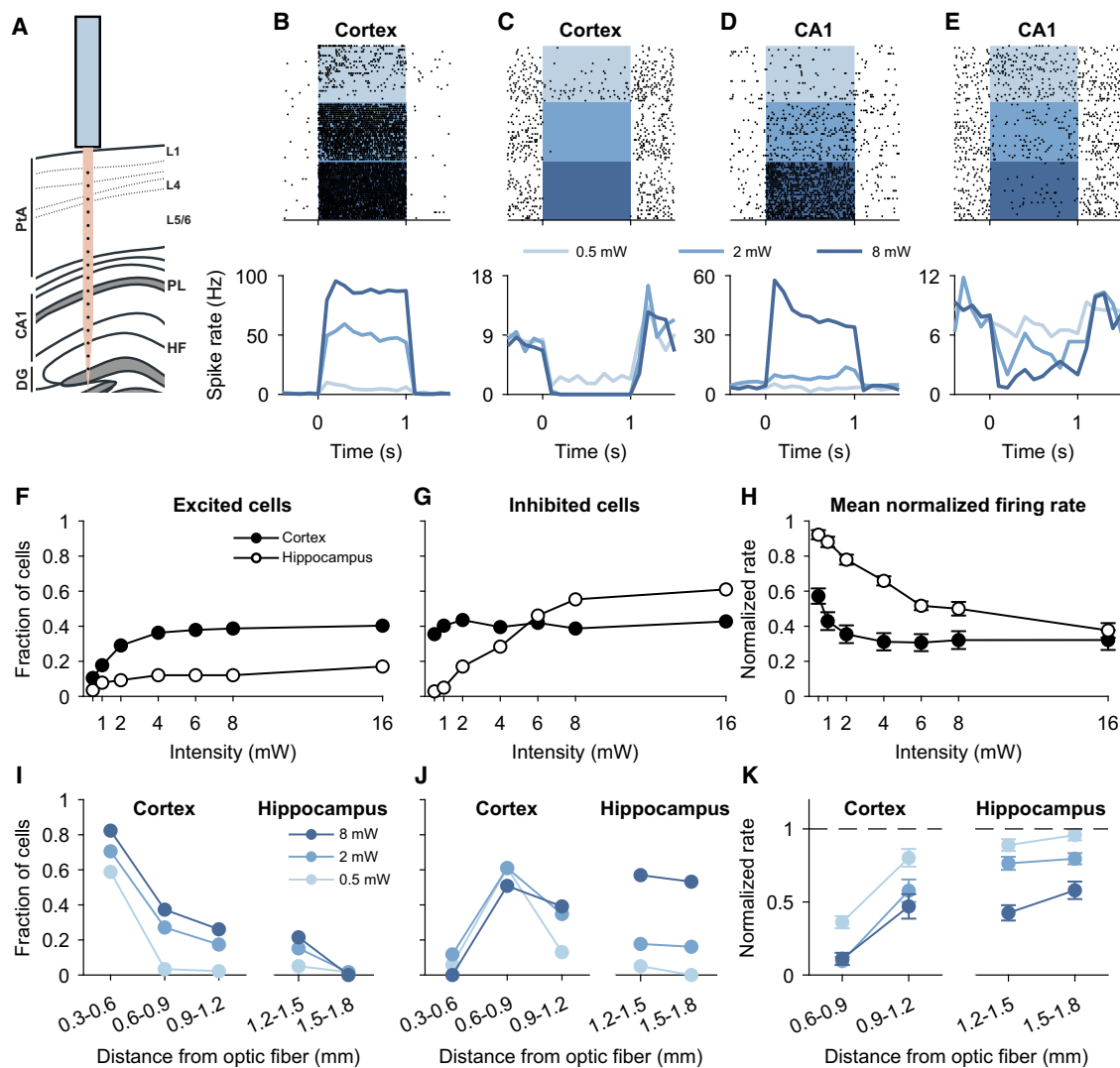


**Figure 2. Light Delivery to the Parietal Cortex in VGAT-ChR2 Mice Causes Neuronal Inhibition Extending to the Subjacent Hippocampus**

(A) Schematic of recording configuration; optic fiber was placed on the surface of the posterior parietal cortex (PtA) and optroprobe recording sites extended through the cortex and into the hippocampus.

(B–E) Raster plots (top) and averaged spike rates (bottom) of example cells recorded in cortex (B and C), and hippocampal CA1 (D and E) showing excitation (B and D) and inhibition (C and E) to 1-s light pulses of different intensities.

(F and G) Fraction of cells in cortex and hippocampus that were significantly excited (F) or inhibited (G) at different light intensities.

(H) Normalized firing rates of putative excitatory neurons in cortex and hippocampus as a function of light intensity. Firing rates decreased in both structures with increasing light intensity.

(I–K) Fraction of excited (I) and inhibited (J) cells and normalized firing rates (K) in the cortex and hippocampus as a function of light intensity and distance from the optic fiber. Firing rates were significantly decreased in the hippocampus at distances greater than 1.2 mm from the optic fiber. Error bars represent the mean  $\pm$  SEM over neurons.

before, the location of the optroprobe was later verified using electrophysiological signatures of the different hippocampal layers (Figure S2).

Across the population of recorded cortical neurons ( $n = 129$ ), we observed cells that were excited (Figure 2B) or inhibited (Figure 2C) by light stimulation. As in the hippocampus, excited cells in the cortex responded with a short latency to light pulses (Figures S3G–S3L) and had a narrower waveform (Figures S4G–S4I), suggesting they were most likely VGAT-positive inhibitory inter-

neurons. Notably, excited and inhibited neurons could also be observed in the subjacent dHPC ( $n = 141$  neurons; Figures 2D–2G). Although the strength of inhibition of putative excitatory neurons was overall higher in the cortex (Figure 2H;  $p < 0.0001$ , main effect of area in an area X intensity ANOVA), significant inhibition was nonetheless observed at all intensities in dHPC (sign-rank test of normalized firing rates, all  $p < 0.0005$ ). An intensity of 6 mW was sufficient to attenuate the firing of dHPC neurons by approximately 50% (normalized firing

rates,  $0.52 \pm 0.02$ ), and the intensity required for maximal inhibition in the cortex (4 mW; normalized rates in cortex,  $0.31 \pm 0.05$ ) reduced firing rates in the dHPC by approximately a third (normalized rates,  $0.66 \pm 0.02$ ). At the highest intensity, the strength of inhibition was similar in the two regions (Figure 2H; cortex:  $0.32 \pm 0.05$ ; dHPC:  $0.38 \pm 0.04$ ). As before, we quantified neural responses during light stimulation as a function of distance from the optic fiber (Figures 2I–2K). This revealed an overall decrease in the strength of inhibition with increasing distance, which was nonetheless still significant more than 1.2 mm below the optic fiber, where hippocampal neurons were recorded (Figure 2K; 1.2–1.5 mm, all  $p < 0.0007$ ; 1.5–1.8 mm,  $p < 0.0001$  for intensities  $>1$  mW; sign-rank test). Taken together, these results extend our initial findings (Figure 1) by demonstrating that inhibition can extend to subjacent subcortical areas when attempting to silence the cortex in VGAT-ChR2 mice.

### Light Delivered to the Somatosensory Cortex of VGAT-ChR2 Mice Can Inhibit Neuronal Activity in the Underlying Striatum

Like the hippocampus, the striatum occupies a large fraction of the brain immediately below the cortex in rodents. To examine the extent to which the striatum might be affected when light is delivered to the cortex in VGAT-ChR2 mice, we performed recordings with the optic fiber of the optoprobe located at the surface of the primary somatosensory cortex so that recording sites spanned the entire cortical depth and also extended into the striatum (Figure 3A; recording position a). Across the population of cortical neurons ( $n = 130$  from 3 mice), we again observed both excited (Figure 3B) and inhibited cells, whose fraction gradually increased with increasing light intensity (Figures 3F and 3G). In contrast, none of the recorded striatal neurons were excited by light stimulation (Figure 3F; 0/32 cells at 16 mW). Strikingly, however, many striatal neurons showed inhibition in response to light stimulation (Figures 3C and 3G). Even at the lowest intensity of 0.5 mW, almost a third of striatal neurons were inhibited (Figure 3G; 10/32 neurons;  $p < 0.001$ , binomial test), which was similar to the percentage observed in the cortex (47/130;  $p = 0.68$ , Fisher's exact test). It is likely that the striatal neurons we recorded were spiny projection neurons that comprise  $\sim 95\%$  of the population and do not appear to express ChR2, although they are GABAergic (see Discussion). Analysis of normalized firing rates of these putative projection neurons furthermore revealed significant inhibition at all intensities (Figure 3H; all  $p < 0.0015$  for intensities  $> 0.5$  mW, sign-rank test), ranging from approximately 20% (0.5 mW;  $0.80 \pm 0.05$ ) to 50% (16 mW;  $0.48 \pm 0.08$ ) reduction in firing, although inhibition strength was overall lower than in the cortex (effect of area in an area X intensity ANOVA,  $p < 0.0001$ ).

Analysis of neuronal responses as a function of distance from the optic fiber (Figures 3I–3K) revealed that inhibition decreased with increasing distance but was nonetheless significant at 1.4–1.7 mm, corresponding to striatal recording sites (Figure 3K;  $p < 0.0015$  for intensities of 0.5 mW and higher). Thus, similar to what we observed in the LP thalamus, robust inhibition was observed in the striatum despite a relative lack of putative GABAergic interneurons activated by light stimulation.

Histological examination revealed that, similar to what we observed in LP thalamus and consistent with previous reports (Guo et al., 2014), ChR2 expression was relatively low in the striatum, although some ChR2-positive cells could be identified and ChR2-positive axonal terminals were also clearly visible (Figures S1E and S1G).

Because of the relatively greater thickness of the somatosensory cortex, in the abovementioned recordings only a few recording sites of the optoprobe extended into the striatum. In order to sample more striatal neurons, we therefore performed additional recordings after lowering the optoprobe until the tip of the optic fiber was 0.5 mm below the brain surface (recording position b in Figure 3A). The distance from the optic fiber to the striatum was thus comparable to its distance from the dHPC in the previous experiment (Figure 2). Again, we observed many excited cells in the cortex (Figure 3L; 32 out of 68 cells at 16 mW; binomial test,  $p < 0.0001$ ) but not in the striatum (Figure 3L; 4 out of 110 cells at 16 mW). Indeed, a sharp drop in the number of excited cells was apparent as soon as the optoprobe entered the striatum (Figure 3L). Nonetheless, more than half of striatal neurons (65/110 at 16 mW) were inhibited by light delivery (Figures 3E and 3M), and significant inhibition of putative projection neurons could be observed at all distances, including the furthest striatal recording sites (Figure 3N; 1.4–1.7 mm from optic fiber,  $p < 0.002$  for intensities  $>0.5$  mW; sign-rank test of normalized firing rates). Finally, we advanced the optoprobe until the optic fiber sat at the top of the striatum and observed neuronal inhibition extending throughout its entire dorsoventral extent (Figure S5). Taken together, these results demonstrate that despite weak opsin expression in the striatum of VGAT-ChR2 mice robust silencing of striatal neurons is nevertheless possible, even when light is delivered to the overlying cortex at relatively low intensities.

### Neuronal Silencing in VGAT-ChR2 Mice Is Spatially Extensive and Varies with Distance in a Non-monotonic Manner

Across multiple cortical and subcortical brain regions, we consistently found that light stimulation in VGAT-ChR2 mice caused neuronal inhibition extending far from the light source. In order to examine the spatial spread of inhibition in more detail, we next combined the data from the different regions and also included neurons that were not included in the previous analyses ( $n = 1,252$  neurons; see STAR Methods). As before, we quantified the fraction of excited and inhibited neurons, as well as normalized firing rates of putative excitatory and projection neurons, as a function of light intensity and distance from the optic fiber (Figures 4A–4C). Similar to what could be observed for individual brain regions (Figures 1, 2, and 3), analysis of the combined dataset at a finer spatial resolution revealed that although inhibition strength varied with distance (Figure 4C; ANOVA of normalized firing rates by distance,  $p < 0.0001$ ), it did so in a non-monotonic manner. Unexpectedly, inhibition was not strongest closest to the optic fiber (0.2–0.4 mm away) but rather at a distance of 0.4–0.6 mm. This was confirmed both by comparing normalized firing rates (Figure 4C; main effect of distance in a distance X intensity ANOVA,  $p < 0.0001$ ; rank-sum test,  $p < 0.0001$  for all intensities;  $n = 58$  and 88

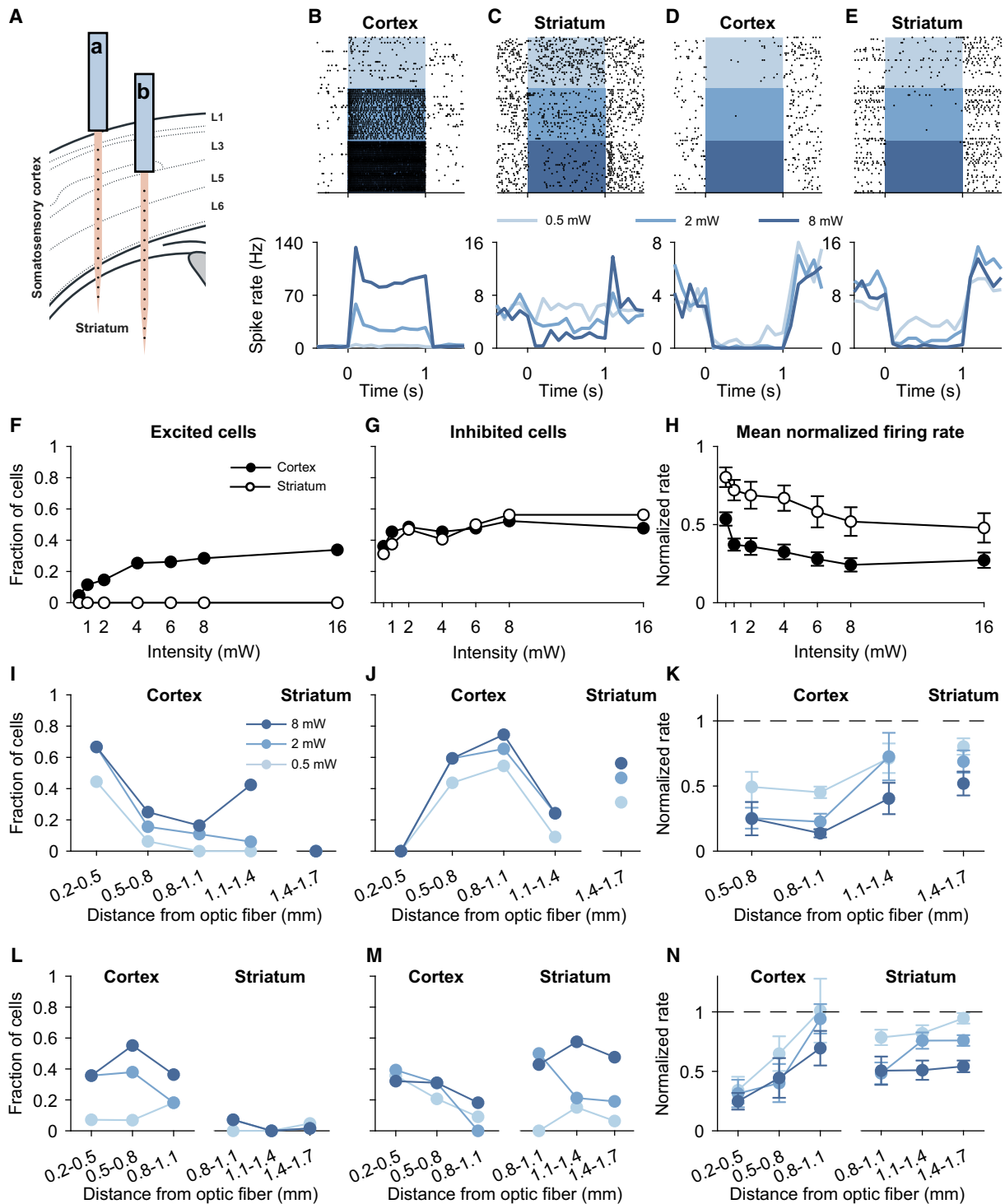


**Figure 3. Light Delivered to the Somatosensory Cortex of VGAT-ChR2 Mice Can Inhibit Neuronal Activity in the Underlying Striatum**

(A) Schematic of recording positions. Optoprobe was positioned so that the optic fiber was either on the brain surface (a) or 500  $\mu\text{m}$  below (b); recording sites spanned the somatosensory cortex and the underlying striatum.

(B–E) Raster plots (top) and averaged spike rates (bottom) of example cells for recording position a (B and C) and b (D and E). Cortical neurons were either excited (B) or inhibited (D), whereas striatal cells displayed only inhibition (C and E).

(F–H) Fraction of cells in cortex and striatum that were excited (F) or inhibited (G) and normalized firing rates of putative excitatory (cortex) and projection neurons (striatum) (H) as a function of light intensity with optic fiber in position a.

(legend continued on next page)

neurons for the 0.2- to 0.4- and 0.4- to 0.6-mm bins, respectively) as well as the proportion of inhibited neurons at these two locations (Figure 4B; Fisher's exact test,  $p < 0.01$  for intensities  $< 8$  mW; ratios calculated from a total of 80 and 134 neurons at the two locations). In contrast, the proportion of excited neurons did not differ at these two locations (Figure 4A; Fisher's exact test,  $p > 0.35$  for all intensities). Weaker inhibition closer to the optic fiber was also observed when we restricted our analysis to more homogeneous populations of neurons from the hippocampal PL or deep layers of the cortex (Figure S6). One possible explanation for these results could be that due to the horizontal scattering of light in brain tissue (Yizhar et al., 2011), a larger population of inhibitory interneurons is recruited further below the light source (Figure S6C; see also Discussion).

At distances greater than 0.6 mm from the optic fiber, inhibition gradually decreased in strength (Figure 4C; main effect of distance on normalized firing rates in a distance X intensity ANOVA,  $p < 0.0001$ ) but remained significant even at 1.6–1.8 mm, the furthest distance we examined (normalized firing rates,  $p < 0.0001$  for all intensities, sign-rank test). At this distance, the proportion of excited neurons was also significant (binomial test;  $p < 0.05$  for intensities  $> 2$  mW, corrected for multiple comparisons). We also confirmed that neurons recorded far from the optic fiber ( $\geq 1.2$  mm) could be activated at a short latency, indicating direct activation by light (Figures S7A–S7F). To further summarize how inhibition strength varies as a function of light intensity and distance, we calculated for each light intensity the maximum distance at which it caused a specific amount of inhibition (Figure 4D). This revealed, for example, that a reduction in firing rate of at least 50% (corresponding to normalized firing rates of 0.5 or lower) was achieved up to a distance of 1.4–1.6 mm for intensities of 8 mW or higher, whereas a reduction of at least 30% could be achieved up to 0.8–1.0 mm with the lowest intensity of 0.5 mW. Taken together, these results demonstrate that light delivery in VGAT-ChR2 mice can cause spatially extensive neuronal silencing even at relatively low light intensities.

### Contribution of Long-Range Inhibitory Projections to Neuronal Silencing

Although inhibitory interneurons mostly target other neurons in their immediate vicinity, they can also send long-range projections to other brain regions (reviewed in Caputi et al., 2013). This raises the possibility that the inhibition we observed in brain areas far away from the optic fiber in VGAT-ChR2 mice might have been caused by the recruitment of long-range inhibitory interneurons in overlying brain regions. Notably, several cortical regions send inhibitory projections to the striatum (Jinno and Kosaka, 2004; Melzer et al., 2017; Rock et al., 2016), which could have contributed to the striatal silencing we observed when delivering light to the somatosensory cortex (Figure 3). To test the contribution of long-range inhibitory projections, we therefore expressed ChR2 in inhibitory interneurons in the somato-

sensory cortex of VGAT-Cre mice (Figure 5A; see STAR Methods). We then delivered blue light to the cortical surface while simultaneously recording in the cortex ( $n = 523$  neurons from 4 mice) as well as the underlying striatum ( $n = 777$  neurons from 4 mice) as before (Figure 5A). Robust ChR2 expression was observed in the somatosensory cortex, and ChR2-positive axons could also be seen in the underlying striatum (Figure 5B, right). Similar to VGAT-ChR2 mice, we observed many excited and inhibited neurons in the cortex (Figures 5C, 5D, 5G, and 5H). In the striatum, inhibition in response to blue light could clearly be observed in some neurons (Figure 5F), but they constituted only a small fraction of the overall population (Figure 5H; 7% or 57/777 neurons at 16 mW). Accordingly, average normalized firing rates in the striatum differed only marginally from baseline (Figures 5I and 5L; normalized rates  $0.95 \pm 0.01$  at 8 mW;  $p < 0.006$  for intensities  $> 2$  mW, sign-rank test). These results stand in contrast to the robust striatal inhibition we observed in VGAT-ChR2 mice when delivering light to the overlying cortex (Figure 3) and suggest that activation of corticostriatal inhibitory interneurons alone is not sufficient to cause strong silencing in the underlying striatum.

An alternative possibility is that inhibition in the striatum, as well as in other regions far from the light source, was caused by optogenetic activation of local interneurons and/or axon terminals. Supporting this possibility, neurons excited by light stimulation could be observed as far as 1.7 mm away from the optic fiber in VGAT-ChR2 mice, including in the striatum (Figures 4A and S7A–S7F). Furthermore, activation of corticostriatal interneurons was not necessary for striatal silencing because this could also be achieved when the optic fiber was directly above the striatum (Figures S5A–S5C). To examine this in more detail, we compared the strength of silencing when the optic fiber was either on top of the striatum or on top of the overlying cortex, as well as when it was 500  $\mu\text{m}$  below the cortical surface. Specifically, we compared neuronal responses to light delivered from these optic fiber locations when the estimated light intensity at the neurons' location was the same (Figure S7G; Stujenske et al., 2015; see STAR Methods). This revealed that light delivery from the two locations resulted in comparable levels of inhibition in the striatum (Figure S7H). In the same manner, we compared inhibition in hippocampal PL neurons when the optic fiber was either on top of the hippocampus (Figure 1C) or the overlying cortex (Figure 2A). This also revealed comparable inhibition of PL neurons from the two locations (Figure S7I). These results are consistent with direct activation of local ChR2-positive interneurons contributing to inhibition far from the light source in VGAT-ChR2 mice.

### Viral Expression of an Inhibitory Opsin Enables Robust and Region-Selective Neuronal Silencing

Our results suggest that achieving spatially restricted neuronal silencing when optogenetically activating interneurons in VGAT-ChR2 mice may be challenging, even when using low

(I–K) Fraction of excited cells (I), inhibited cells (J) cells and normalized firing rates (K) as a function of distance from the optic fiber (in position a) for different light intensities; inhibition is observed in both cortex and underlying striatum but excitatory responses are only observed in cortex.

(L–N) Same as in (I)–(K) but with optic fiber 500  $\mu\text{m}$  below brain surface (recording position b). Excitation is largely restricted to the cortex, but inhibition extends to striatum at a distance of 1.4–1.7 mm from optic fiber. Error bars represent the mean  $\pm$  SEM over neurons.

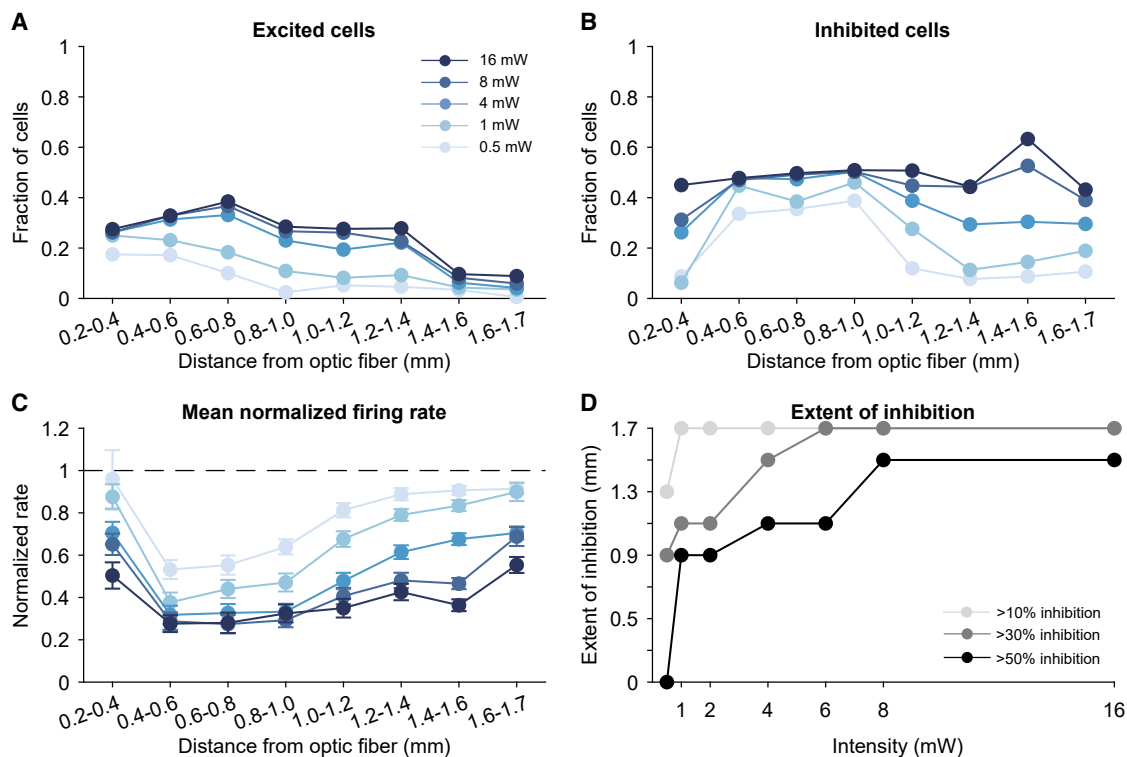


**Figure 4. Spatially Extensive Neuronal Silencing in VGAT-ChR2 Mice**

(A and B) Fraction of cells from all recorded brain regions combined that were excited (A) or inhibited (B) as a function of distance from the optic fiber and light intensity.

(C) Normalized firing rates of all recorded putative excitatory and projection neurons as a function of distance from optic fiber. Inhibition was strongest approximately 0.5 mm below the optic fiber and extended to a distance of 1.7 mm.

(D) Spatial extent of different inhibition levels as a function of light intensity. Each line shows how far from the optic fiber a specific amount of inhibition can be achieved with a given light intensity. Error bars represent the mean  $\pm$  SEM over neurons.

light intensities. Another widely used strategy for optogenetic silencing is to express a hyperpolarizing opsin in a region of interest by targeted injection of a viral expression construct (Kim et al., 2017; Yizhar et al., 2011). In theory, this should restrict neuronal silencing to the area of opsin expression. To compare this approach with silencing in VGAT-ChR2 mice, we virally expressed the proton pump archaerhodopsin T (ArchT; Han et al., 2011) in the dHPC of wild-type mice (Figures 6A, 6B, and S1H–S1K; see STAR Methods). We then recorded simultaneously in the dHPC and underlying LP thalamus as previously in VGAT-ChR2 mice (Figure 1) while delivering yellow light pulses (594 nm, 1 s, 0.5–16 mW) to the dHPC (Figure 6C; optic fiber  $483.33 \pm 39.97 \mu\text{m}$  above the PL;  $n = 9$  recording sessions from 4 mice). As expected, the activity of many dHPC neurons in ArchT-expressing mice was inhibited by light delivery (Figures 6D and 6E); at intensities of 1 mW or higher, approximately half of the recorded dHPC neurons ( $n = 439$ ) were significantly inhibited (Figure 6I; 218/439 neurons at 1 mW). The strength of inhibition increased with increasing light intensity (Figure 6J), reaching near-asymptotic levels of an approximately 50% reduction in firing rate at 2 mW (normalized rates,  $0.53 \pm 0.02$ ) and only modestly stronger inhibition at higher intensities ( $0.47 \pm 0.03$  at 16 mW;  $p < 0.0001$  for all intensities, sign-rank test).

In contrast to the robust neuronal silencing we observed in the hippocampus, inhibition was virtually absent in the subjacent LP thalamus of ArchT-expressing mice (Figures 6F and 6G). Few neurons were inhibited by light delivery (Figure 6I; 0/37 at 8 mW, 3/37 at 16 mW), and firing rates were overall not significantly different from baseline (Figure 6J;  $p > 0.05$  at all intensities, sign-rank test of normalized firing rates, corrected for multiple comparisons). These results contrast with the pronounced inhibition observed in LP neurons when delivering light to the hippocampus of VGAT-ChR2 mice (Figures 1I and 1J). To examine in more detail the spatial specificity of silencing in ArchT-expressing mice, we quantified normalized firing rates as a function of neurons' distance from the PL (Figure 6K). This revealed that neuronal inhibition was strongest in the region immediately surrounding the PL (0.1 mm above and below), where it resulted in near-complete silencing (normalized rates,  $0.05 \pm 0.01$  at 16 mW). Significant inhibition could be observed between 0.3 mm above and 0.9 mm below the PL, corresponding approximately to the CA1 and dentate gyrus subregions (Figure 6K). In contrast, no inhibition was observed beyond this region (Figure 6K;  $p > 0.05$ , sign-rank test of normalized firing rates, corrected for multiple comparisons), confirming hippocampus-specific silencing. Finally, we examined how the strength of inhibition of neurons

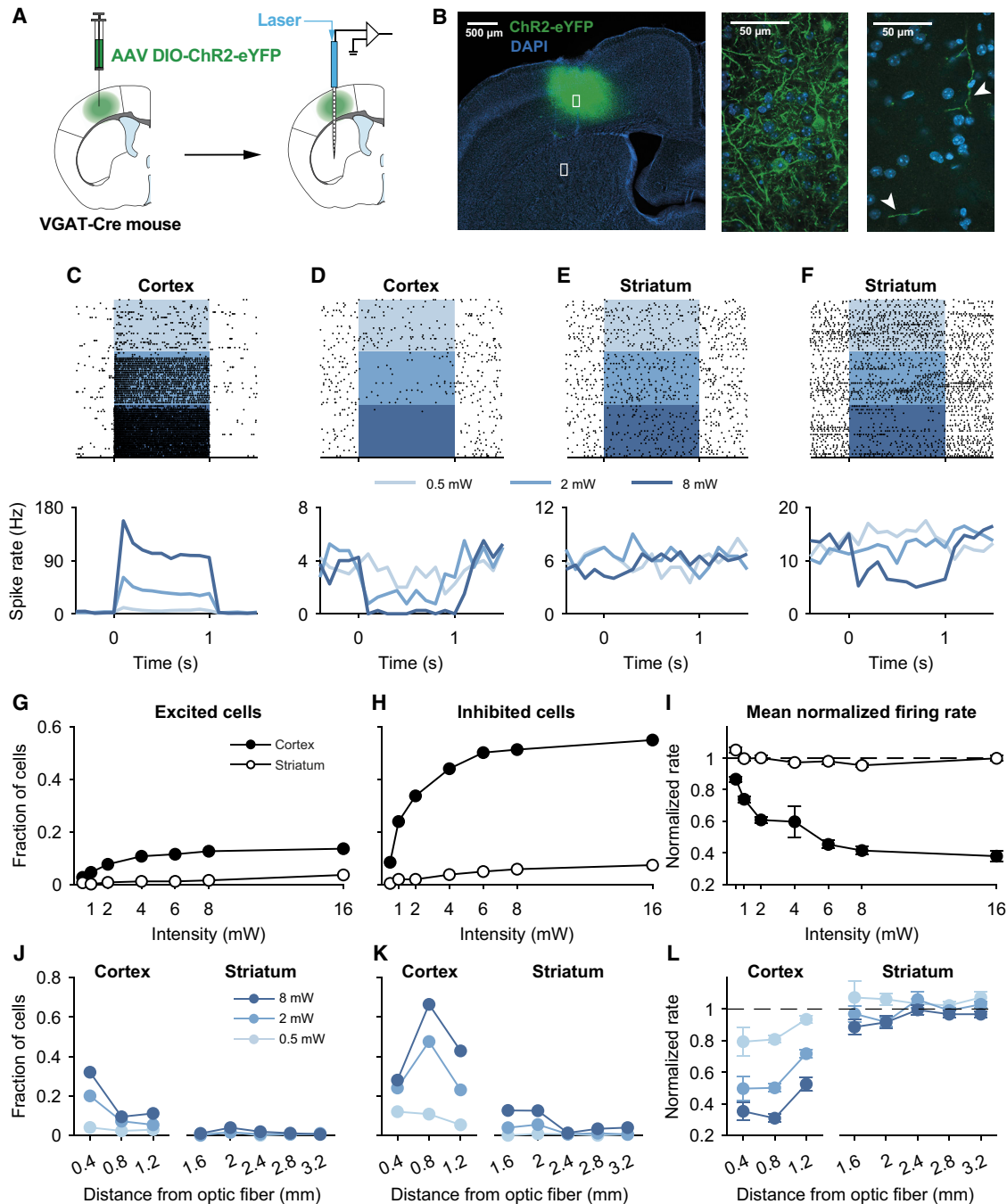


**Figure 5. Contribution of Long-Range Inhibitory Projections to Neuronal Silencing**

(A) ChR2 was expressed selectively in interneurons in the somatosensory cortex. Blue light was then delivered to the cortical surface while recording simultaneously in the cortex and underlying striatum.

(B) Left, histological image showing ChR2 expression in the somatosensory cortex. White boxes define areas shown at a higher magnification from cortex (middle) and striatum (right). White arrows indicate ChR2-positive axon terminals in striatum.

(C–F) Raster plots (top) and averaged spike rates (bottom) of example neurons during light stimulation. Robust excitation and inhibition was seen in the cortex (C and D), whereas only a few neurons showed inhibition in the striatum (E and F).

(G and H) Fraction of cells in cortex and striatum that were significantly excited (G) or inhibited (H) at different light intensities.

(I) Normalized firing rates of putative projection neurons in cortex and striatum as a function of light intensity.

(J–L) Fraction of excited (J) and inhibited (K) cells and normalized firing rates of putative projection neurons (L) in the cortex and striatum as a function of light intensity and distance from the optic fiber. Tick marks on the x-axes represent the centers of 0.4 mm bins.

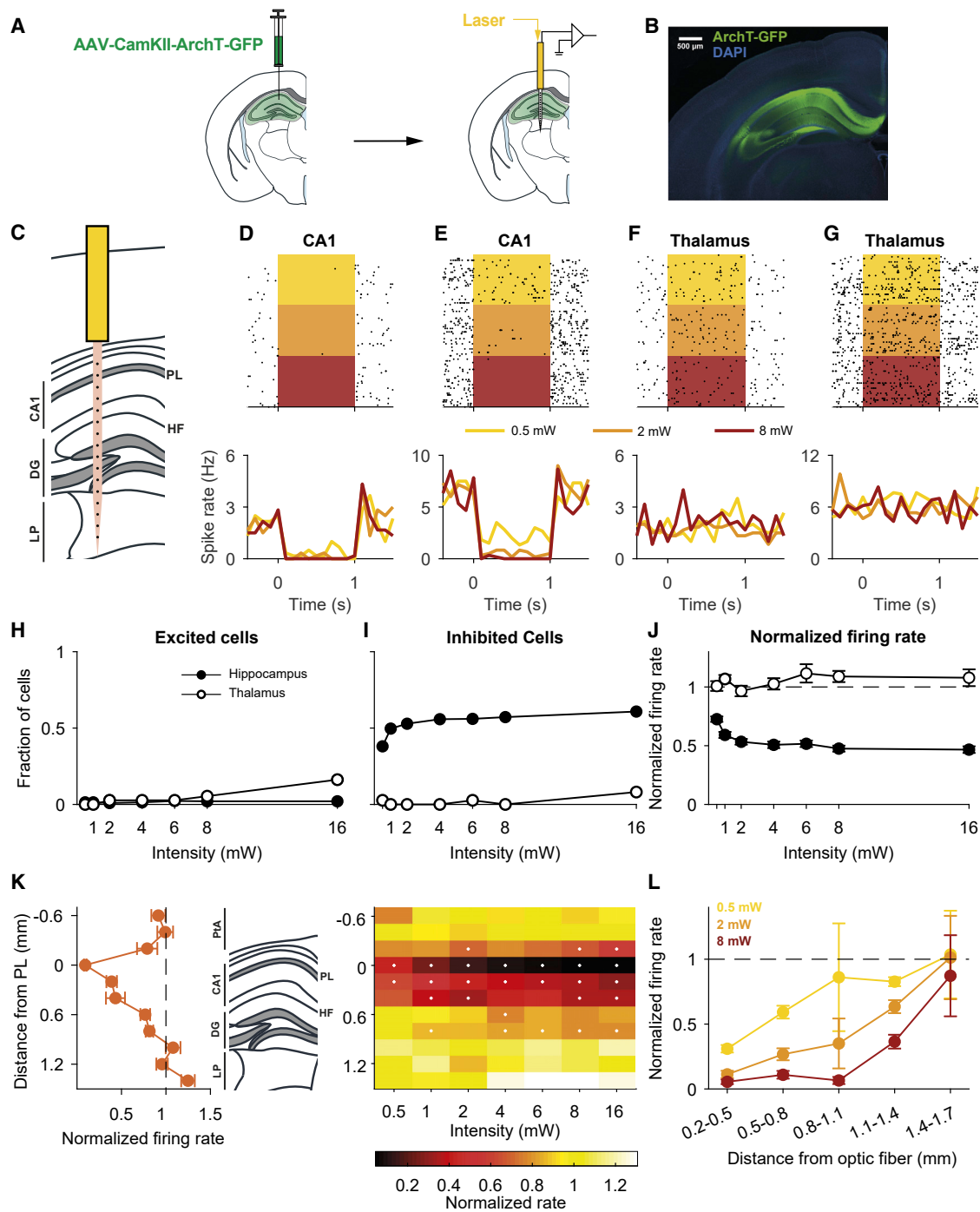


**Figure 6. Viral Expression of an Inhibitory Opsin Enables Robust and Region-Selective Neuronal Silencing**

(A) Schematic of experiment; a virus expressing ArchT-GFP was injected locally into the hippocampus of wild-type mice and yellow light was delivered to hyperpolarize neurons.

(B) Example coronal section showing ArchT-GFP expression restricted to the dHPC.

(C) The optoprobe was positioned so that the optic fiber sat above the CA1 PL; recording sites extended from the hippocampus into the subjacent thalamus.

(D–G) Raster plots (top) and averaged spike rates (bottom) of example cells in hippocampus showing inhibition to light pulses (D and E) and thalamic neurons showing no response (F and G).

(H and I) Fraction of cells recorded in hippocampus and thalamus that were significantly excited (H) or inhibited (I) at different light intensities.

(J) Normalized firing rates as a function of light intensity; firing rates were selectively reduced in the hippocampus but not in the thalamus.

(legend continued on next page)

in the PL region depends on their distance from the optic fiber (Figure 6L). To this end, we also included in our analyses data obtained with the optic fiber placed on the surface of the cortex overlying the dHPC (STAR Methods). As expected, and in contrast to what we observed in VGAT-ChR2 mice, inhibition was strongest for PL neurons located right below the optic fiber. Inhibition strength then decreased with increasing distance (Figure 6L; main effect of distance on normalized firing rates in a distance X intensity ANOVA,  $p < 0.0001$ ) but could nevertheless be observed when the optic fiber was as far as 1.1–1.4 mm away (Figure 6L; sign-rank test of normalized firing rates,  $p < 0.0001$  for all intensities). At this distance, firing rates were reduced by approximately 65% at 8 mW (normalized rates,  $0.36 \pm 0.05$ ). Taken together, these results demonstrate that viral expression of an inhibitory opsin enables neuronal silencing of a spatially restricted region, even when that region is located far from the light source.

### The Influence of Light on Neuronal Activity

Our results demonstrate how light-mediated activation of opsins can be used for neuronal silencing. However, when evaluating the effects of such optogenetic manipulations, one needs to consider the possible influence of light itself on neuronal activity. Indeed, at sufficiently high intensities, light can cause heating of neuronal tissue that, in turn, can alter neuronal firing rates (Owen et al., 2019; Stujenske et al., 2015). To address whether this could have influenced our results, we examined responses to blue or yellow light in wild-type mice without any opsin expression. Light was delivered to the same brain regions at the same intensity and for the same duration as in our experiments in ChR2- and ArchT-expressing animals while recording neuronal activity as before. Across the entire population of recorded neurons, the vast majority (89% or 354/378 neurons;  $n = 2$  mice) were unresponsive to blue light stimulation (Figures S8A, S8C, and S8K). However, approximately 7% of neurons (28/378) displayed significant excitatory responses (Figures S8B, S8D, and S8K). Many of these responses were transient and had a delayed onset (Figures S8B and S8D), suggesting that they were driven by the visual input caused by light stimulation rather than heating of neuronal tissue (Owen et al., 2019; Stujenske et al., 2015). Indeed, excitatory responses were most common in the LP thalamus (15.8% or 6/38 neurons), which is a visual area. In contrast, inhibitory responses to light stimulation were only observed in 4% (16/378) of all neurons. Analysis of normalized firing rates furthermore revealed that across the entire population firing rates were slightly elevated on average (normalized rates,  $1.16 \pm 0.03$  at 16 mW;  $p < 0.00001$ , sign-rank test), although these effects varied depending on the brain region (Figures S8E–S8G). However, in contrast to what would be expected if tissue heating was responsible, the effect of light did not appear to depend on neurons' distance from the optic fiber (Figure S8I). Similar results were obtained when yellow light was delivered to the hippocampus in the

same way as in ArchT-expressing mice (Figures S8H and S8J). Taken together, these results suggest that the effects of light itself did not contribute to the neuronal inhibition we observed in VGAT-ChR2 and ArchT mice, although modest light-induced excitatory responses might have counteracted inhibitory responses in some cases.

## DISCUSSION

### The Spatial Extent of Inhibition in VGAT-ChR2 Mice

VGAT-ChR2 mice, in which neural activity can be inhibited by optogenetically activating GABAergic interneurons, have become a widely used tool for silencing brain regions and testing their causal contribution to behavior (Goard et al., 2016; Guo et al., 2014, 2017; Le Merre et al., 2018; Mathis et al., 2017; Sreenivasan et al., 2016; Wimmer et al., 2015; Zhao et al., 2011). Major advantages of this approach are that virus injections are not required to express inhibitory opsins and multiple brain regions can be silenced in a single animal (Galiñanes et al., 2018; Goard et al., 2016; Guo et al., 2014; Le Merre et al., 2018). However, because ChR2 is expressed in GABAergic interneurons throughout the brain, the intensity of light must be carefully controlled in order to restrict silencing to the region of interest and avoid affecting neighboring structures. Characterizing the spatial extent of inhibition in VGAT-ChR2 mice and how it depends on light intensity as well as distance from the light source is therefore of crucial importance.

To address this, in the current study we attempted to selectively silence three target structures in VGAT-ChR2 mice: the hippocampus, the parietal cortex, and the somatosensory cortex. We delivered light at different intensities to each of these target regions while simultaneously recording neural activity within them as well as in their subjacent structures (the thalamus, hippocampus, and striatum, respectively). In all cases, we found that intensities required for maximal silencing in the target region also caused significant silencing in the subjacent areas, and at higher intensities even resulted in similar levels of inhibition in some cases. More generally, we found that neuronal inhibition could be observed as far as 1.7 mm away from the optic fiber, the furthest distance we examined. Notably, at this distance a reduction in firing rates of approximately 50% could be observed at the highest intensity, suggesting that inhibition can likely extend even further below the light source in VGAT-ChR2 mice. In addition, inhibition can also extend for several millimeters lateral to the light source in these mice (Guo et al., 2014).

These results highlight the importance of carefully controlling light intensities when using VGAT-ChR2 mice, as well as other mouse lines expressing ChR2 in GABAergic interneurons (Madsen et al., 2012), to selectively silence specific brain regions. Notably, our results demonstrate that light delivered to the cortical surface can cause inhibition extending to the

(K) Normalized firing rate of neurons as a function of their position relative to the PL at 4 mW (left) and all light intensities (right). White asterisks indicate a significant decrease of firing rate ( $p < 0.05$ , corrected for multiple comparisons). Diagram in the middle represents the estimated anatomical location of recorded neurons. Inhibition is strongest closest to the PL and restricted to the hippocampus.

(L) Normalized firing rates of cells recorded in the PL as a function of their distance from the optic fiber. Error bars represent the mean  $\pm$  SEM over neurons.

hippocampus and striatum, the two main subcortical structures that lie immediately below the cortex. Even the lowest intensity we tested (0.5 mW, corresponding to a light power density of  $\sim 15$  mW/mm<sup>2</sup>), which is lower than what has typically been used in previous experiments with VGAT-ChR2 mice, resulted in significant inhibition in these subcortical structures (8%–20%, depending on the region). An earlier study found that light delivered to the cortical surface in VGAT-ChR2 mice caused silencing in the cortex but not in the subjacent striatum (Guo et al., 2014). Although the different light delivery method in this study prevents a direct comparison with ours, we suspect that the light intensity in Guo et al. (2014) may have been lower than the lowest intensity we used. Based on the modest striatal inhibition we observed at 0.5 mW, we expect that we might also have been able to achieve more region-selective silencing at lower intensities. However, our data demonstrate that lower intensities will also result in less inhibition in target structures (20%–40% inhibition at 0.5 mW). Thus, silencing using VGAT-ChR2 mice involves a tradeoff between the strength and selectivity of silencing.

#### Factors Influencing the Spatial Extent of Inhibition in VGAT-ChR2 Mice

The spatial extent of inhibition in VGAT-ChR2 mice depends on several factors whose relative contributions are incompletely understood. One key factor is the light scattering properties of brain tissue (Yizhar et al., 2011; Yona et al., 2016), which will cause a gradual attenuation of light intensity with increasing distance from the light source and a corresponding decrease in the recruitment of GABAergic inhibitory interneurons. Consistent with this, we found that the fraction of neurons directly excited by light stimulation (putative interneurons) decreased gradually with increasing distance from the optic fiber. Significant excitatory responses could nonetheless be observed as far as 1.6–1.8 mm away for intensities of 4 mW and higher. Based on the model of Stujenske et al. (2015), 4 mW would result in a light intensity of 0.2–0.7 mW/mm<sup>2</sup> at this distance, which is sufficient to activate ChR2 (Mattis et al., 2011).

Another factor that undoubtedly contributes to the spatial extent of inhibition in VGAT-ChR2 mice are the axonal arborizations of GABAergic interneurons (Pelkey et al., 2017; Tepper et al., 2018; Tremblay et al., 2016). In the cortex, for example, interneurons can inhibit pyramidal neurons located several hundred micrometers away either within the same layer (Fino and Yuste, 2011; Kätzel et al., 2011) or in different layers (Bortone et al., 2014; Kätzel et al., 2011). Inhibition is therefore expected to be more spatially extensive than the recruitment of interneurons. Interneuron arborization patterns may also account for one unexpected aspect of our results, namely that inhibition was strongest not right below the light source but approximately half a millimeter below it (Figures 4B and 4C). We suspect that neurons further away from the light source are more effectively silenced because a larger proportion of their GABAergic input population is recruited by light stimulation. For neurons located further below the optic fiber tip, interneurons that are located above them are more likely to be activated by light; in addition, the horizontal scattering of light in brain tissue increases with increasing distance from the light source (Yizhar et al., 2011),

thus potentially leading to greater recruitment of horizontal inhibitory inputs (Figure S6C). At any rate, these findings highlight how the spatial profile of inhibition in VGAT-ChR2 mice can be highly nonlinear, likely owing to the specific architecture of interneuron networks that are recruited during light stimulation.

In addition to their local projections, there is increasing evidence that GABAergic interneurons can send long-range projections between brain regions (Caputi et al., 2013; Lee et al., 2014; Melzer et al., 2017). Inhibition in regions far from the optic fiber in VGAT-ChR2 mice could, therefore, have been caused by activation of long-range inhibitory neurons in overlying regions closer to the optic fiber. Notably, subpopulations of interneurons in several cortical regions project to the striatum (Jinno and Kosaka, 2004; Melzer et al., 2017; Rock et al., 2016). However, our recordings in mice expressing ChR2 selectively in cortical interneurons do not support a major role of such corticostriatal interneurons in generating the striatal inhibition we observed in VGAT-ChR2 mice when delivering light to the cortex. Nonetheless, it is possible that activation of these neurons had subtler effects on neuronal firing than we could detect. To the best of our knowledge, no long-range inhibitory projections exist that could have contributed to the silencing we observed in the thalamus and hippocampus when delivering light to the hippocampus and cortex, respectively. Generally speaking, however, inhibitory interneurons in these and other structures can send long-range projections to many subcortical and cortical areas (Caputi et al., 2013; Jinno et al., 2007; Melzer et al., 2012; Tremblay et al., 2016). Such projections therefore represent a potential obstacle to spatially restricting inhibition in VGAT-ChR2 mice. Furthermore, there is evidence that some of these projections preferentially target other inhibitory interneurons (Melzer et al., 2012) and may thus cause disinhibition, which could further complicate the interpretation of results from these mice.

In the thalamus and striatum, light stimulation excited few neurons but nevertheless caused robust neuronal silencing. Histological examination revealed relatively few ChR2-positive neurons in these structures, consistent with low numbers of GABAergic interneurons reported in previous studies (Evangeliou et al., 2018; Tepper et al., 2018). It is interesting to note that  $\sim 95\%$  of neurons in the striatum are in fact GABAergic projection neurons, although they do not seem to express ChR2, as suggested by the low ChR2 expression levels in this region (our study; Guo et al., 2014). However, it is possible that the small numbers of excited striatal neurons we observed were GABAergic interneurons, which, although only comprising 3%–4% of the total population, can nonetheless generate robust inhibition in the striatum (Lee et al., 2017). Alternatively, inhibition could have resulted from stimulation of ChR2-positive axon terminals, which can directly generate inhibitory postsynaptic potentials (Zhao et al., 2011) and which were abundant in both the thalamus and striatum. These axon terminals may have partly originated in outside brain regions. Indeed, the striatum and the LP thalamus receive inhibitory input from the cortex (Melzer et al., 2017; Rock et al., 2016) and the thalamic reticular nucleus (Pinault et al., 1995), respectively. Regardless of the mechanism involved, these results suggest that regional variation in ChR2 expression levels may not be a reliable predictor

of the strength of inhibition in individual brain regions of VGAT-ChR2 mice.

### Viral Expression of an Inhibitory Opsin Enables Region-Specific Neuronal Silencing

Another widely used approach for inhibiting neuronal activity is to express light-activated hyperpolarizing opsins in a neuronal population of interest through viral infection. To compare this approach with neuronal silencing in VGAT-ChR2 mice, we virally expressed the proton pump ArchT (Han et al., 2011) in the hippocampus of wild-type mice. Because activation of ArchT directly hyperpolarizes neurons, silencing of neural activity should be restricted to the region of opsin expression. Indeed, in contrast to VGAT-ChR2 mice, we found that ArchT enabled selective silencing of the hippocampus without inhibiting the subjacent LP thalamus, regardless of the light intensity used. This suggests that when using inhibitory opsins, light can be used at intensities sufficient to reach maximal inhibition without affecting subjacent structures, assuming opsin expression is regionally restricted. The lack of an effect in the thalamus in ArchT mice also argues against the possibility that the inhibition of thalamic neurons in VGAT-ChR2 mice was caused indirectly by removal of excitatory input to this region (Otchy et al., 2015).

The strength of neuronal inhibition also varied with distance from the light source in ArchT mice but did so in a more linear fashion than in VGAT-ChR2 mice. We could also demonstrate that neurons in the hippocampal PL of ArchT-expressing mice could be silenced when the optic fiber was positioned as much as 1.1–1.4 mm above (see also Weible et al., 2014). One implication of these results is that placing the light source slightly above the region of opsin expression may allow a larger volume to be silenced because the horizontal spread of light increases with increasing distance from the light source (Yizhar et al., 2011). These results also demonstrate that controlling light intensity is equally important when using transgenic mouse lines with brain-wide expression of inhibitory opsins (Madisen et al., 2012; Weible et al., 2014). It should also be kept in mind that activation of proton pumps, such as ArchT and other Arceorhodopsin variants, which transport protons out of the cell, can lead to alkalization of the intracellular space (El-Gaby et al., 2016; Mahn et al., 2016) that, in turn, can have unintended physiological consequences.

### Concluding Remarks

Controlling the spatial extent of inhibition is critical for the precise optogenetic manipulation of neural activity. Our findings suggest guidelines for designing and interpreting experiments using VGAT-ChR2 mice as well as other mouse lines expressing ChR2 in GABAergic interneurons (Madisen et al., 2012). Provided that light intensities are carefully chosen, VGAT-ChR2 and similar mouse lines can be of value, especially for testing the behavioral role of multiple brain regions in a single animal. However, for testing the role of single brain regions, especially if they are relatively small, viral expression of inhibitory opsins should be strongly considered as an alternative strategy in order to ensure spatial selectivity. VGAT-ChR2 mice are also a valuable tool for optogenetically identifying inhibitory interneurons (Schneider et al., 2014) as well as for studying inhibitory

synaptic transmission *in vitro* (Xie and Manis, 2014). Finally, we note that although the key experimental parameters (light wavelength and intensities, diameter and numerical aperture of optic fiber) were the same in our study as in the majority of previous studies, changing these parameters might yield quantitatively different results. Similarly, our results may not generalize to all other areas due to regional variability in opsin expression in VGAT-ChR2 mice (Zhao et al., 2011) as well as differences in interneuron arborization patterns. Characterizing the spatial spread of inhibition and examining whether it extends to structures beyond those targeted for silencing should therefore be an essential part of future studies using VGAT-ChR2 and similar mouse lines.

### STAR★METHODS

Detailed methods are provided in the online version of this paper and include the following:

- KEY RESOURCES TABLE
- LEAD CONTACT AND MATERIALS AVAILABILITY
- EXPERIMENTAL MODEL AND SUBJECT DETAILS
- METHOD DETAILS
  - Surgical procedures
  - Optogenetic silencing and electrophysiological recording
  - Histology
  - Detection and clustering of neuronal spikes
  - Anatomical localization of recording sites
- QUANTIFICATION AND STATISTICAL ANALYSIS
  - Analysis of firing rate modulation
- DATA AND CODE AVAILABILITY

### SUPPLEMENTAL INFORMATION

Supplemental Information can be found online at <https://doi.org/10.1016/j.celrep.2019.09.049>.

### ACKNOWLEDGMENTS

This work was supported by Priority Program 1665 (SI 1942/4-1) and Collaborative Research Center 1193 (subproject B03) of the DFG. We would like to thank Jasmine Sonntag, Felicia Müller-Braun, and Thomas Wulf for histological and technical assistance; Sevil Duvarci for comments on the manuscript; and Annalena Babi for help with illustrations.

### AUTHOR CONTRIBUTIONS

Conceptualization and Experimental Design, S.S.B. and T.S.; Methodology, S.S.B. and B.P.R.; Software, S.S.B., B.P.R., and T.S.; Investigation, S.S.B.; Formal Analysis, S.S.B. and T.S.; Writing – Original Draft, T.S. and S.S.B.; Writing – Review & Editing, S.S.B., B.P.R., and T.S.; Funding Acquisition, T.S.

### DECLARATION OF INTERESTS

The authors declare no competing interests.

Received: April 5, 2019

Revised: August 5, 2019

Accepted: September 18, 2019

Published: October 29, 2019

## REFERENCES

- Al-Juboori, S.I., Dondzillo, A., Stubblefield, E.A., Felsen, G., Lei, T.C., and Klug, A. (2013). Light scattering properties vary across different regions of the adult mouse brain. *PLoS One* 8, e67626.
- Aravanis, A.M., Wang, L.-P., Zhang, F., Meltzer, L.A., Mogri, M.Z., Schneider, M.B., and Deisseroth, K. (2007). An optical neural interface: in vivo control of rodent motor cortex with integrated fiberoptic and optogenetic technology. *J. Neural Eng.* 4, S143–S156.
- Asrican, B., Augustine, G.J., Berglund, K., Chen, S., Chow, N., Deisseroth, K., Feng, G., Gloss, B., Hira, R., Hoffmann, C., et al. (2013). Next-generation transgenic mice for optogenetic analysis of neural circuits. *Front. Neural Circuits* 7, 160.
- Azimipour, M., Atry, F., and Pashaie, R. (2015). Effect of blood vessels on light distribution in optogenetic stimulation of cortex. *Opt. Lett.* 40, 2173–2176.
- Bortone, D.S., Olsen, S.R., and Scanziani, M. (2014). Translaminar inhibitory cells recruited by layer 6 corticothalamic neurons suppress visual cortex. *Neuron* 82, 474–485.
- Buzsáki, G. (2002). Theta oscillations in the hippocampus. *Neuron* 33, 325–340.
- Buzsáki, G., Buhl, D.L., Harris, K.D., Csicsvari, J., Czéh, B., and Morozov, A. (2003). Hippocampal network patterns of activity in the mouse. *Neuroscience* 116, 201–211.
- Caputi, A., Melzer, S., Michael, M., and Monyer, H. (2013). The long and short of GABAergic neurons. *Curr. Opin. Neurobiol.* 23, 179–186.
- Chow, B.Y., Han, X., Dobry, A.S., Qian, X., Chuong, A.S., Li, M., Henninger, M.A., Belfort, G.M., Lin, Y., Monahan, P.E., and Boyden, E.S. (2010). High-performance genetically targetable optical neural silencing by light-driven proton pumps. *Nature* 463, 98–102.
- El-Gaby, M., Zhang, Y., Wolf, K., Schwiening, C.J., Paulsen, O., and Shipton, O.A. (2016). Archærodopsin Selectively and Reversibly Silences Synaptic Transmission through Altered pH. *Cell Rep.* 16, 2259–2268.
- Evangelio, M., García-Amado, M., and Clascá, F. (2018). Thalamocortical Projection Neuron and Interneuron Numbers in the Visual Thalamic Nuclei of the Adult C57BL/6 Mouse. *Front. Neuroanat.* 12, 27.
- Fino, E., and Yuste, R. (2011). Dense inhibitory connectivity in neocortex. *Neuron* 69, 1188–1203.
- Galiñanes, G.L., Bonardi, C., and Huber, D. (2018). Directional Reaching for Water as a Cortex-Dependent Behavioral Framework for Mice. *Cell Rep.* 22, 2767–2783.
- Goard, M.J., Pho, G.N., Woodson, J., and Sur, M. (2016). Distinct roles of visual, parietal, and frontal motor cortices in memory-guided sensorimotor decisions. *eLife* 5, e13764.
- Guo, Z.V., Li, N., Huber, D., Ophir, E., Gutnisky, D., Ting, J.T., Feng, G., and Svoboda, K. (2014). Flow of cortical activity underlying a tactile decision in mice. *Neuron* 81, 179–194.
- Guo, Z.V., Inagaki, H.K., Daie, K., Druckmann, S., Gerfen, C.R., and Svoboda, K. (2017). Maintenance of persistent activity in a frontal thalamocortical loop. *Nature* 545, 181–186.
- Han, X., Chow, B.Y., Zhou, H., Klapoetke, N.C., Chuong, A., Rajimehr, R., Yang, A., Baratta, M.V., Winkle, J., Desimone, R., and Boyden, E.S. (2011). A high-light sensitivity optical neural silencer: development and application to optogenetic control of non-human primate cortex. *Front. Syst. Neurosci.* 5, 18.
- Jinno, S., and Kosaka, T. (2004). Parvalbumin is expressed in glutamatergic and GABAergic corticostriatal pathway in mice. *J. Comp. Neurol.* 477, 188–201.
- Jinno, S., Klausberger, T., Marton, L.F., Dalezios, Y., Roberts, J.D.B., Fuentelba, P., Bushong, E.A., Henze, D., Buzsáki, G., and Somogyi, P. (2007). Neuronal diversity in GABAergic long-range projections from the hippocampus. *J. Neurosci.* 27, 8790–8804.
- Johansson, J.D. (2010). Spectroscopic method for determination of the absorption coefficient in brain tissue. *J. Biomed. Opt.* 15, 057005.
- Kätzel, D., Zemelman, B.V., Buetfering, C., Wölfel, M., and Miesenböck, G. (2011). The columnar and laminar organization of inhibitory connections to neocortical excitatory cells. *Nat. Neurosci.* 14, 100–107.
- Kim, C.K., Adhikari, A., and Deisseroth, K. (2017). Integration of optogenetics with complementary methodologies in systems neuroscience. *Nat. Rev. Neurosci.* 18, 222–235.
- Le Merre, P., Esmaeili, V., Charrière, E., Galan, K., Salin, P.-A., Petersen, C.C.H., and Crochet, S. (2018). Reward-Based Learning Drives Rapid Sensory Signals in Medial Prefrontal Cortex and Dorsal Hippocampus Necessary for Goal-Directed Behavior. *Neuron* 97, 83–91.e5.
- Lee, A.T., Vogt, D., Rubenstein, J.L., and Sohal, V.S. (2014). A class of GABAergic neurons in the prefrontal cortex sends long-range projections to the nucleus accumbens and elicits acute avoidance behavior. *J. Neurosci.* 34, 11519–11525.
- Lee, K., Holley, S.M., Shobe, J.L., Chong, N.C., Cepeda, C., Levine, M.S., and Masmanidis, S.C. (2017). Parvalbumin Interneurons Modulate Striatal Output and Enhance Performance during Associative Learning. *Neuron* 93, 1451–1463.e4.
- Ludwig, K.A., Miriani, R.M., Langhals, N.B., Joseph, M.D., Anderson, D.J., and Kipke, D.R. (2009). Using a common average reference to improve cortical neuron recordings from microelectrode arrays. *J. Neurophysiol.* 101, 1679–1689.
- Madisen, L., Mao, T., Koch, H., Zhuo, J.-M., Berenyi, A., Fujisawa, S., Hsu, Y.-W.A., Garcia, A.J., 3rd, Gu, X., Zanella, S., et al. (2012). A toolbox of Cre-dependent optogenetic transgenic mice for light-induced activation and silencing. *Nat. Neurosci.* 15, 793–802.
- Mahn, M., Prigge, M., Ron, S., Levy, R., and Yizhar, O. (2016). Biophysical constraints of optogenetic inhibition at presynaptic terminals. *Nat. Neurosci.* 19, 554–556.
- Mathis, M.W., Mathis, A., and Uchida, N. (2017). Somatosensory Cortex Plays an Essential Role in Forelimb Motor Adaptation in Mice. *Neuron* 93, 1493–1503.e6.
- Mattis, J., Tye, K.M., Ferenczi, E.A., Ramakrishnan, C., O’Shea, D.J., Prakash, R., Gunaydin, L.A., Hyun, M., Fenno, L.E., Gradinaru, V., et al. (2011). Principles for applying optogenetic tools derived from direct comparative analysis of microbial opsins. *Nat. Methods* 9, 159–172.
- Melzer, S., Michael, M., Caputi, A., Eliava, M., Fuchs, E.C., Whittington, M.A., and Monyer, H. (2012). Long-range-projecting GABAergic neurons modulate inhibition in hippocampus and entorhinal cortex. *Science* 335, 1506–1510.
- Melzer, S., Gil, M., Koser, D.E., Michael, M., Huang, K.W., and Monyer, H. (2017). Distinct Corticostriatal GABAergic Neurons Modulate Striatal Output Neurons and Motor Activity. *Cell Rep.* 19, 1045–1055.
- Mitzdorf, U. (1985). Current source-density method and application in cat cerebral cortex: investigation of evoked potentials and EEG phenomena. *Physiol. Rev.* 65, 37–100.
- Montgomery, S.M., Betancur, M.I., and Buzsáki, G. (2009). Behavior-dependent coordination of multiple theta dipoles in the hippocampus. *J. Neurosci.* 29, 1381–1394.
- Nicholson, C., and Freeman, J.A. (1975). Theory of current source-density analysis and determination of conductivity tensor for anuran cerebellum. *J. Neurophysiol.* 38, 356–368.
- Otchy, T.M., Wolff, S.B.E., Rhee, J.Y., Pehlevan, C., Kawai, R., Kempf, A., Gobes, S.M.H., and Ölveczky, B.P. (2015). Acute off-target effects of neural circuit manipulations. *Nature* 528, 358–363.
- Owen, S.F., Liu, M.H., and Kreitzer, A.C. (2019). Thermal constraints on in vivo optogenetic manipulations. *Nat. Neurosci.* 22, 1061–1065.
- Paxinos, G., and Franklin, K.B.J. (2007). *The Mouse Brain in Stereotaxic Coordinates* (Elsevier Science).
- Pelkey, K.A., Chittajallu, R., Craig, M.T., Tricoire, L., Wester, J.C., and McBain, C.J. (2017). Hippocampal GABAergic Inhibitory Interneurons. *Physiol. Rev.* 97, 1619–1747.

- Pinault, D., Bourassa, J., and Deschênes, M. (1995). Thalamic reticular input to the rat visual thalamus: a single fiber study using biocytin as an anterograde tracer. *Brain Res.* 670, 147–152.
- Resulaj, A., Ruediger, S., Olsen, S.R., and Scanziani, M. (2018). First spikes in visual cortex enable perceptual discrimination. *eLife* 7, e34044.
- Rock, C., Zurita, H., Wilson, C., and Apicella, A.J. (2016). An inhibitory cortico-striatal pathway. *eLife* 5, e15890.
- Rossant, C., Kadir, S.N., Goodman, D.F.M., Schulman, J., Hunter, M.L.D., Saleem, A.B., Grosmark, A., Belluscio, M., Denfield, G.H., Ecker, A.S., et al. (2016). Spike sorting for large, dense electrode arrays. *Nat. Neurosci.* 19, 634–641.
- Schneider, D.M., Nelson, A., and Mooney, R. (2014). A synaptic and circuit basis for corollary discharge in the auditory cortex. *Nature* 513, 189–194.
- Sreenivasan, V., Esmaili, V., Kiritani, T., Galan, K., Crochet, S., and Petersen, C.C.H. (2016). Movement Initiation Signals in Mouse Whisker Motor Cortex. *Neuron* 92, 1368–1382.
- Stujenske, J.M., Spellman, T., and Gordon, J.A. (2015). Modeling the Spatio-temporal Dynamics of Light and Heat Propagation for In Vivo Optogenetics. *Cell Rep.* 12, 525–534.
- Tepper, J.M., Koós, T., Ibanez-Sandoval, O., Tecuapetla, F., Faust, T.W., and Assous, M. (2018). Heterogeneity and Diversity of Striatal GABAergic Interneurons: Update 2018. *Front. Neuroanat.* 12, 91.
- Tremblay, R., Lee, S., and Rudy, B. (2016). GABAergic Interneurons in the Neocortex: From Cellular Properties to Circuits. *Neuron* 91, 260–292.
- Weible, A.P., Moore, A.K., Liu, C., DeBlander, L., Wu, H., Kentros, C., and Wehr, M. (2014). Perceptual gap detection is mediated by gap termination responses in auditory cortex. *Curr. Biol.* 24, 1447–1455.
- Wiegert, J.S., Mahn, M., Prigge, M., Printz, Y., and Yizhar, O. (2017). Silencing Neurons: Tools, Applications, and Experimental Constraints. *Neuron* 95, 504–529.
- Wimmer, R.D., Schmitt, L.I., Davidson, T.J., Nakajima, M., Deisseroth, K., and Halassa, M.M. (2015). Thalamic control of sensory selection in divided attention. *Nature* 526, 705–709.
- Xie, R., and Manis, P.B. (2014). GABAergic and glycinergic inhibitory synaptic transmission in the ventral cochlear nucleus studied in VGAT channelrhodopsin-2 mice. *Front. Neural Circuits* 8, 84.
- Yizhar, O., Fenno, L.E., Davidson, T.J., Mogri, M., and Deisseroth, K. (2011). Optogenetics in neural systems. *Neuron* 71, 9–34.
- Yona, G., Meitav, N., Kahn, I., and Shoham, S. (2016). Realistic Numerical and Analytical Modeling of Light Scattering in Brain Tissue for Optogenetic Applications(1,2,3). *eNeuro* 3, ENEURO.0059-15.2015.
- Zhang, F., Wang, L.-P., Brauner, M., Liewald, J.F., Kay, K., Watzke, N., Wood, P.G., Bamberg, E., Nagel, G., Gottschalk, A., and Deisseroth, K. (2007). Multimodal fast optical interrogation of neural circuitry. *Nature* 446, 633–639.
- Zhao, S., Ting, J.T., Atallah, H.E., Qiu, L., Tan, J., Gloss, B., Augustine, G.J., Deisseroth, K., Luo, M., Graybiel, A.M., and Feng, G. (2011). Cell type-specific channelrhodopsin-2 transgenic mice for optogenetic dissection of neural circuitry function. *Nat. Methods* 8, 745–752.

## STAR★METHODS

### KEY RESOURCES TABLE

| REAGENT or RESOURCE                                     | SOURCE                                 | IDENTIFIER  |
|---|--|---|
| <b>Antibodies</b>                                       |  |   |
| Anti-GFP (rabbit)                                       | Thermo Fischer Scientific              | Cat# A-11122; RRID: AB_221569   |
| Anti-rabbit-Alexa Fluor 488 (goat)                      | Thermo Fischer Scientific              | Cat# A-11008; RRID: AB_143165   |
| <b>Bacterial and Virus Strains</b>                      |  |   |
| rAAV5/CamKII-ArchT-GFP                                  | UNC Vector Core                        | Lot #AV4606B  |
| rAAV5/Ef1a-DIO-hChr2(H134R)-eYFP                        | UNC Vector Core                        | Lot #AV4313Z  |
| <b>Chemicals, Peptides, and Recombinant Proteins</b>    |  |   |
| Dil   | Life Technologies                      | Lot #1646663  |
| DAPI  | Thermo Fischer Scientific              | Cat# D1306; RRID: AB_2629482  |
| <b>Experimental Models: Organisms/Strains</b>           |  |   |
| Mouse: VGAT-ChR2-EYFP; Slc32a1-COP4*H134R/EYFP          | The Jackson Laboratory                 | Stock No. 014548  |
| Mouse: VGAT-ires-cre; Slc32a1 <sup>tm2(cre)Lowl/J</sup> | The Jackson Laboratory                 | Stock No. 028862  |
| Mouse: C57BL/6N   | Charles River Laboratories             | N/A   |
| <b>Software and Algorithms</b>                          |  |   |
| RHD2000 Interface software                              | Intan Technologies                     | <a href="http://intantech.com/downloads.html">http://intantech.com/downloads.html</a> |
| Klusta  | <a href="#">Rossant et al., 2016</a>   | <a href="https://github.com/kwikteam/klusta">https://github.com/kwikteam/klusta</a>   |
| Monte Carlo simulation                                  | <a href="#">Stujenske et al., 2015</a> | N/A   |
| MATLAB 2017b  | MathWorks                              | <a href="https://de.mathworks.com">https://de.mathworks.com</a>                       |
| <b>Other</b>  |  |   |
| Optic fiber   | Thorlabs                               | #CFML12L10 or #CFML22L20  |
| 16-channel silicon probe (100 μm spacing)               | ATLAS Neuroengineering                 | #E16-100-S1-L10   |
| 32-channel silicon probe (50 μm spacing)                | ATLAS Neuroengineering                 | #E32-50-S1-L6   |
| 32-channel silicon probe (100 μm spacing)               | ATLAS Neuroengineering                 | #E32-100-S1-L6  |
| 473 nm diode laser                                      | Omicron Laserage                       | LuxX 473-100  |
| 594 nm DPSS laser                                       | Omicron Laserage                       | LightHUB®-1 594 nm 100 mW   |

### LEAD CONTACT AND MATERIALS AVAILABILITY

Further information and requests for resources and reagents should be directed to and will be fulfilled by the Lead Contact, Torfi Sigurdsson ([sigurdsson@em.uni-frankfurt.de](mailto:sigurdsson@em.uni-frankfurt.de)). This study did not generate new unique reagents.

### EXPERIMENTAL MODEL AND SUBJECT DETAILS

We used 5 male transgenic VGAT-ChR2-EYFP mice, which express the H134R variant of Chr2 fused with EYFP under the control of the vesicular GABA transporter promoter (Slc32a1-COP4\*H134R/EYFP; the Jackson Laboratory, Stock No. 014548; [Zhao et al., 2011](#)), 4 male transgenic VGAT-ires-Cre mice (Slc32a1<sup>tm2(cre)Lowl/J</sup>; the Jackson Laboratory, Stock No. 028862), and 6 male wild-type C57BL/6N mice (Charles River Laboratories). All animals were 3-5 months of age at the beginning of the experiments and were kept in a ventilated animal container on a 12h light/dark cycle. Experiments were performed during the light period. All procedures described here were approved by the local animal care committee (Regierungspräsidium Darmstadt).

### METHOD DETAILS

#### Surgical procedures

Preceding all surgeries, mice were anesthetized in a chamber filled with 3%–4% isoflurane, placed in a stereotaxic frame and injected with carprofen (4 mg/kg, subcutaneously) and dexamethasone (2 mg/kg, subcutaneously) for reducing pain and inflammation, atropine (0.1 mg/kg, intraperitoneal) to decrease mucus secretions and Ringer's solution (1 ml, subcutaneously) as fluid replacement.

During the surgery, anesthesia was maintained with an isoflurane concentration of 1%–2% (in oxygen at a flow rate of 0.35 l/min), which was regularly adjusted based on the monitored breathing rate. Body temperature was maintained at 37°C with a heating blanket placed under the animal.

We injected 4 wild-type C57BL/6N mice with rAAV5-CamKII-ArchT-GFP (titer  $\sim 7.5 \times 10^{12}$  vg/ml, UNC Vector Core) bilaterally into the dorsal hippocampus (dHPC). To this end, the skull was exposed and small craniotomies were made above the dHPC (AP:  $-2.0$  mm, ML:  $-/+1.5$  mm relative to bregma). A 35 gauge needle attached to a syringe (NANOFIL 10 $\mu$ l, World Precision Instruments) was then inserted to a depth of 1.40–1.45 mm below brain surface. With a microsyringe pump controller (UltraMicroPump III, World Precision Instruments), we injected 1  $\mu$ L of the viral construct in each hemisphere at a constant speed of 100 nl/min. After the injection, the Hamilton syringe was left in place for an additional 10 min to allow viral diffusion from the tip. The scalp was then sutured closed using a medical sewing kit. Mice were allowed to recover for one week. Time between viral injection and neuronal recording was 4–5 weeks.

Four VGAT-Cre mice were injected with rAAV5/Ef1a-DIO-hChR2(H134R)-eYFP (titer  $\sim 3.2 \times 10^{12}$  vg/ml, UNC Vector Core) unilaterally into the somatosensory cortex (S1). A small craniotomy was made above S1 (AP:  $+0.25$  mm, ML:  $-2.0$  mm relative to bregma) and a 35 gauge needle attached to a syringe was first inserted to a depth of  $-0.75$  mm below brain surface for the first injection and then retracted to a depth of  $-0.35$  mm below brain surface for the second injection. At each injection site, we injected 250 nL at a speed of 30 nl/min as described before. Time between viral injection and neuronal recording was 5–6 weeks.

For mounting of the head post, mice were anesthetized and placed on the stereotaxic frame as described above. After exposing the skull, the coordinates for future craniotomies were marked on the skull overlying left posterior parietal association cortex (PtA; AP:  $-2.0$  mm, ML:  $-1.5$  mm; for recordings in PtA and dHPC) and/or left primary somatosensory cortex (S1; AP:  $+0.25$  mm, ML:  $-2.0$  mm; for recordings in S1 and striatum) with a waterproof pen. Then, a stainless-steel head post (Luigs and Neumann) was cemented to the skull above the cerebellum. The area overlying PtA and/or S1 was left free of cement but covered with a silicone elastomer (Kwik-Sil; #600009, World Precision Instruments). Skull screws (# 4-009122000014010, Mercateo) were inserted over the frontal cortex and cerebellum to serve as reference and ground, respectively, and to provide anchoring support for the head post. Animals were allowed to recover for one week before further experimental procedures.

### Optogenetic silencing and electrophysiological recording

Following recovery from head post implantation, mice were habituated to head-fixation on a daily basis with sessions of increasing length (15–60 min). The head-fixed setup was inside a sound attenuating chamber and dimly illuminated by a red or an infrared LED. Mice were placed on a foam-covered plastic platform and head-fixed by inserting the head post into a matching head post holder (Luigs and Neumann). Two plastic walls on the sides of the platform gave the mouse additional support and restrained movement. Animals were given a liquid reward every 20–30 s, consisting of 3–6  $\mu$ L of 10% sucrose solution. Rewards were delivered from a spout in front of animals by opening a solenoid valve (003-0218-900, Parker Hannifin) between the spout and a liquid reservoir above it. Animals licked the spout to consume the reward, which was detected by a custom-built infrared emitter and detector on either side of the reward spout.

Following habituation to head-fixation (typically 3–4 days) the animals underwent a brief procedure to prepare a craniotomy over PtA or S1. In VGAT-ChR2 mice, ArchT-injected mice and two naive mice, a craniotomy was made over the PtA for cortical and hippocampal recordings. In three of the five VGAT-ChR2 mice and in the two naive mice a craniotomy was also made above S1 for cortical and striatal recordings. In the four VGAT-Cre mice, a craniotomy was made above S1 for cortical and striatal recordings. Animals were anesthetized with isoflurane, placed in a stereotaxic frame, and the Kwik-Sil was removed from the skull. A small craniotomy ( $\sim 500$   $\mu$ m radius) was then made around the previously marked coordinates (see above) in the skull overlying the left PtA or left S1. After opening the craniotomy, with the dura left intact, it was sealed with Kwik-Sil.

The following day, the animals were head-fixed as described before. The Kwik-Sil was removed and a custom-made silicon optoprobe (Atlas Neuroengineering) was inserted through the craniotomy. The optoprobe consisted of an optic fiber (#CFML12L10 or #CFML22L20, Thorlabs, 200  $\mu$ m diameter core, 0.39 NA) mounted on a 16- or 32-channel silicon probe (#E16-100-S1-L10, #E32-50-S1-L6 or #E32-100-S1-L6, Atlas Neuroengineering) so that the tip of the optic fiber was 200  $\mu$ m above the first recording site. The spacing between the recording sites was 100  $\mu$ m or 50  $\mu$ m. In VGAT-ChR2, ArchT-injected and naive mice, we used probes in which the entire distance from the optic fiber tip to the deepest recording site was 1.70 or 1.75 mm. For VGAT-Cre mice, we used a longer 32-channel probe (100  $\mu$ m spacing) with a distance of 3.3 mm between the optic fiber tip and deepest recording site. The optoprobe was advanced slowly through the brain tissue with a micromanipulator (SM-8, Luigs and Neumann) to its target location. In VGAT-ChR2, ArchT-injected and naive mice, recordings were made with the optic fiber of the optoprobe right above the hippocampus ( $\sim 1.0$  mm below brain surface; [Figures 1 and 6](#); [Figure S8](#)) and at the surface of PtA cortex ([Figures 2 and 6](#)). In VGAT-ChR2, VGAT-Cre and naive mice, recordings were also made with the optic fiber at or 0.5 mm below the surface of S1 cortex ([Figures 3, 5, and S8](#)) or just above the striatum ( $\sim 1.5$  mm below brain surface; [Figure S5](#)). For recordings including the dHPC the position of the optoprobe was subsequently confirmed using electrophysiological signatures of the hippocampal layers ([Figure S2](#); see below).

Following final placement of the optoprobe and a brief waiting period (5–10 min), neural activity was recorded while 1 s pulses of either 473 nm (for VGAT-ChR2, VGAT-Cre and naive mice) or 594 nm (for ArchT-expressing and naive mice) light were delivered through the optic fiber using a laser (LuxX 473-100 and LH-1, respectively, Omicron-Laserage). Light pulses were delivered at 7 different intensities (0.5, 1, 2, 4, 6, 8 and 16 mW, measured at the fiber tip) in a repeating cycle (30–60 repetitions per intensity)

with an inter-stimulus interval of 1 or 2 s. The timing and intensity of light pulses was controlled with a microcontroller (Arduino Uno, Arduino) and a custom-built digital-analog converter connected to the laser.

Electrophysiological signals were high-pass filtered (500–7500 Hz), digitized at 30 kHz using a digitizing headstage (RHD2132 Amplifier Board, Intan Technologies) and acquired using a USB interface board (RHD2000, Intan Technologies). The latter also recorded the time stamps of laser onsets and offsets based on TTL pulses delivered by the microcontroller that controlled the laser. At each recording site, we also recorded spontaneous broadband activity (1–7500 Hz, 20 kHz sampling rate) for 5 min without light stimulation. This was used for subsequent offline confirmation of electrode location (see below; [Figure S2](#)). During the session animals received rewards at random intervals as described above in order to maintain their alertness. At the end of each recording session, the silicon probe was removed from the brain, after which the craniotomy was carefully rinsed with artificial cerebrospinal fluid and closed with Kwik-Sil. Before the last recording session, the silicon probe was coated with a fluorescent dye (Dil, Life Technologies) to assist with subsequent histological confirmation of the recording position.

### Histology

After the last recording session, all animals were anesthetized with Na-pentobarbital and perfused transcardially with 4% paraformaldehyde, 15% picric acid in PBS (pH 7.4). After post-fixation overnight, brains were cut on a vibratome at a thickness of 80  $\mu\text{m}$  per brain section. Brain sections of VGAT-Cre animals were processed with GFP immunohistochemistry using standard procedures. Briefly, the sections were washed three times in PBS and then incubated in a carrier solution (1% horse serum, 0.5% Triton X-100% and 0.2% BSA in PBS) containing the primary antibody anti-GFP (#A11122, 1:1000, Thermo Fisher Scientific) overnight at room temperature. On the following day, the sections were washed in PBS and incubated overnight in carrier solution containing the secondary antibody anti-rabbit Alexa Fluor 488 (#A11008, 1:750, Thermo Fisher Scientific). After washing in PBS, the sections were incubated in DAPI solution (Thermo Fisher Scientific, #D1306; 1  $\mu\text{g}/\text{mL}$  in PBS) for five minutes, washed in PBS and then mounted on microscope slides. Brain slices of VGAT-ChR2 mice, ArchT-injected mice and naive mice were washed in PBS and incubated in DAPI solution for five minutes. After washing in PBS, the sections were mounted on microscope slides. Electrode placement (based on Dil-labeled electrode tracks) and virus expression was verified in all animals using a confocal microscope (Eclipse90i, Nikon). In ArchT mice, virus expression was restricted to the dorsal hippocampus ([Figures S1H–S1K](#)). In VGAT-Cre mice, ChR2 expression was restricted to the cortex but in some animals a thin layer ( $\sim 100 \mu\text{m}$ ) of ChR2 expression could be observed right below the corpus callosum in the dorsal-most tip of the striatum. However, normalized firing rates in the striatum of these animals during light delivery were comparable to what we observed in the animal without any striatal expression.

### Detection and clustering of neuronal spikes

To analyze neuronal spiking, we first performed common average referencing on all electrode sites ([Ludwig et al., 2009](#)). Spikes were then detected and sorted into single-unit clusters using klusta (<https://github.com/kwikteam/klusta>; [Rossant et al., 2016](#)). Briefly, spikes were detected as spatiotemporally connected components using a double-threshold flood fill algorithm (SpikeDetekt) and clustered into single-units based on their waveform features. Initial clustering was done by an automated masked expectation-maximization algorithm (Masked KlustaKwik). This was followed by manual refinement based on visual inspection of the spike waveforms as well as the auto- and cross-correlograms of each cluster using phy Kwik GUI. All subsequent analyses were performed using custom-written scripts in MATLAB (MATLAB 2017b, MathWorks). A neurons' location was estimated to correspond to the recording site of the silicon probe where the amplitude of its waveform was largest. This was subsequently used to assign neurons to different brain regions (see below).

### Anatomical localization of recording sites

To determine the anatomical position of each electrode site in recordings that included the dHPC ([Figures 1, 2, and 6](#)), we examined several electrophysiological signatures that characterize the different layers of the hippocampus ([Figure S2](#)). Specifically, we examined the variation in ripple (150–250 Hz) and theta (4–12 Hz) oscillations in the local field potential (LFP), as well as multi-unit activity, across recording sites ([Buzsáki, 2002](#); [Buzsáki et al., 2003](#)). First, the broadband recordings were down-sampled to 2 kHz. We then extracted ripple oscillations by filtering the broadband signal between 150 and 250 Hz and quantified ripple power across recording sites. For analysis of theta oscillations, we first filtered the broadband signal between 4 and 12 Hz and identified the channel with the largest theta oscillations. This channel was used to construct a theta peak-triggered average of theta oscillation recorded at all channels ([Montgomery et al., 2009](#)). Current source density analysis (CSD; [Mitzdorf, 1985](#); [Nicholson and Freeman, 1975](#)) was then performed on the averaged theta waveforms. Multi-unit firing rates were calculated for each channel based on the detected spikes (see above) after excluding noise clusters. With these features we determined the location of two anatomical regions in the hippocampus: the pyramidal layer (PL) of the CA1 region and the hippocampal fissure (HF), which separates CA1 from the dentate gyrus (DG). The PL was identified as the recording site showing a local maximum of ripple power and high multi-unit firing rates ([Buzsáki et al., 2003](#)). From CSD analysis of theta oscillations we furthermore identified current sources and sinks in the PL and HF, a gradual theta phase reversal between the two areas, and a theta amplitude maximum at the HF ([Buzsáki, 2002, 2003](#); [Montgomery et al., 2009](#)).

For every recording site we calculated its distance to the PL and HF. The position of each neuron relative to these landmarks was then obtained by determining the recording site where its spike waveform was largest. This information was used to assign each neuron to a particular area based on the mouse brain atlas ([Paxinos and Franklin, 2007](#)). Neurons recorded more than 250  $\mu\text{m}$  above

the hippocampal pyramidal layer were classified as PtA cells. Neurons recorded 250  $\mu\text{m}$  above the PL or lower, but above the HF, were classified as CA1 cells. Neurons recorded below the HF, but with a distance of less than 1.10 mm below the PL were classified as dentate gyrus cells. Neurons at 1.10 mm or more below the PL were identified as thalamic cells. For recordings in S1 and striatum, the neurons' location was determined based on the recording site where its waveform was largest and the micromanipulator travel depth. Neurons recorded less than 1.4 mm below brain surface were classified as S1 cells. Neurons recorded at a depth of 1.4 mm or more were classified as striatal cells.

Recordings including the hippocampus were furthermore included for analysis based on the estimated position of the optic fiber relative to the PL: for recordings in hippocampus and thalamus (Figure 1 and 6), sessions were included where the optic fiber was 200–600  $\mu\text{m}$  (VGAT-ChR2 mice) or 200–650  $\mu\text{m}$  (ArchT-expressing mice) above the PL. For recordings in the cortex and hippocampus (Figure 2), sessions were included where the optic fiber was 1200–1550  $\mu\text{m}$  above the PL. For examining inhibition in ArchT-injected mice as a function of distance from the PL (Figure 6K), the optic fiber was 200–1000  $\mu\text{m}$  above the PL. For examining responses to light stimulation across brain regions (Figure 4), all cells were included for analysis. For analysis of responses as a function of distance from the optic fiber, the ratio of excited/inhibited neurons and normalized firing rates were only calculated for distance bins containing at least 4 neurons.

## QUANTIFICATION AND STATISTICAL ANALYSIS

### Analysis of firing rate modulation

We first examined whether a neuron was excited or inhibited by light stimulation by asking whether its firing rate during the first 500 ms after light onset was higher or lower, respectively, than its firing rate in the 500 ms immediately before light onset. This was examined separately for each light intensity (Wilcoxon signed-rank test,  $p < 0.05$ , corrected for multiple comparisons). In order to quantify the strength of inhibition we calculated the normalized firing rate by dividing the mean firing in the first 500 ms after laser onset by the mean baseline firing in the 500 ms before laser onset. For VGAT-ChR2 and VGAT-Cre mice, this analysis was only performed for putative excitatory or projection neurons, which we defined as neurons that were not significantly excited by light delivery at any intensity and thus likely not VGAT-positive. For recordings in cortex, hippocampus and thalamus these neurons are referred to as putative excitatory neurons. In the striatum, these neurons were mostly likely the spiny projection neurons which comprise  $\sim 95\%$  of the neuronal population, and are thus referred to as putative projection neurons. To further support this classification, we quantified two features of the spike waveform of each neuron recorded in VGAT-ChR2 mice: The spike width, defined as the time from the valley to the return to baseline after the peak, and the ratio between peak and valley amplitudes. This revealed that excited neurons had a narrower waveform and larger peak-to-valley ratio, suggesting they were likely inhibitory interneurons (Figure S4).

To calculate latencies of excitatory and inhibitory responses (Figure S3), we first calculated a peri-stimulus time histogram (PSTH) for each neuron and light intensity representing firing rates 0–100 ms after light onset in 5 ms bins. We then generated surrogate PSTHs by calculating the average firing of the same neuron during the 100 ms preceding light onset (5 ms bins) from a random subset of 60 trials. This was repeated 10,000 times to create a distribution of firing rates that would be expected from random (spontaneous) firing. The firing rate in each bin of the actual PSTH was then compared against this random distribution. We identified when the actual firing rate was higher (for excited cells) or lower (for inhibited cells) than 95% of the random distribution in at least 3 consecutive bins. The response latency was defined as the time between laser onset and the first of these bins.

For comparing responses of neurons recorded at different distances from the optic fiber and with the optic fiber in different positions (Figures S7G–S7I), we estimated for each light intensity delivered from the optic fiber the resulting light intensity at the neurons' position. This requires estimating the attenuation of light through brain tissue, for which we used a Monte Carlo Simulation of photon scattering (MonteCarloLight; Stujenske et al., 2015). The simulation is based on measurements of the optical properties of brain tissue (Johansson, 2010) and takes into account the radius and numerical aperture of the optic fiber, as well as the light wavelength. The simulation results in an estimate of relative light intensity as a function of vertical and horizontal distance from the optic fiber tip. The light intensity at each neuron's location was calculated by averaging the relative intensity at its vertical position from the optic fiber tip within a horizontal radius of 0.1 mm from the fiber center.

All statistical analysis was performed in MATLAB (MATLAB 2017b, MathWorks). Applied statistical tests are described in the results section for each figure. Figures show either absolute numbers or the mean  $\pm$  SEM over the number of cells included in the respective analysis.

## DATA AND CODE AVAILABILITY

Original source data and code are available upon request to the Lead Contact.

**Cell Reports, Volume 29**

**Supplemental Information**

**The Spatial Extent of Optogenetic  
Silencing in Transgenic Mice Expressing  
Channelrhodopsin in Inhibitory Interneurons**

**Susanne Stefanie Babl, Brian Paul Rummell, and Torfi Sigurdsson**

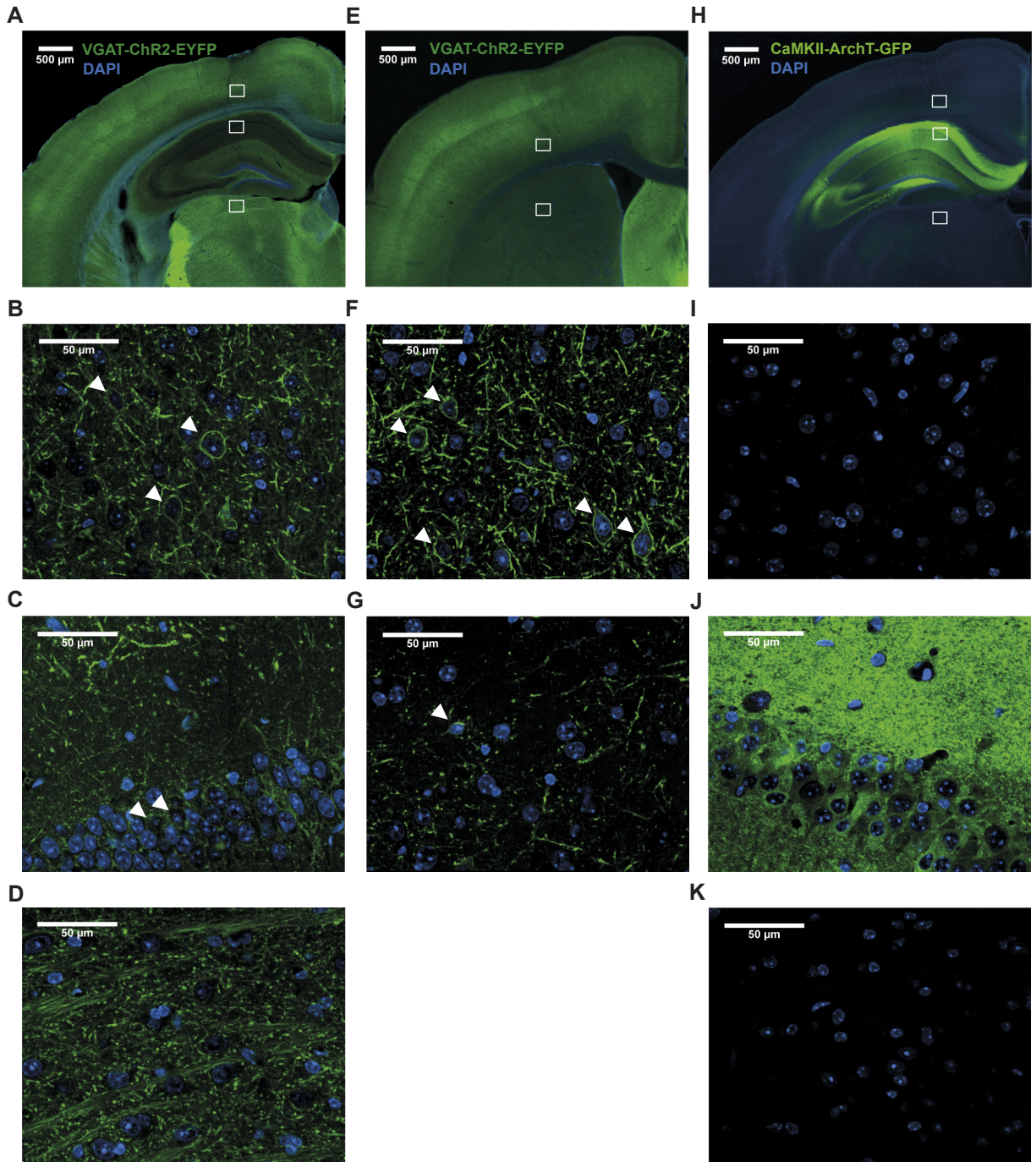


**Figure S1, Opsin expression in brain areas that were recorded from VGAT-ChR2 and ArchT-expressing mice, related to Figures 1-3 and 6.** *A*, Coronal brain section from a VGAT-ChR2 mouse showing ChR2-EYFP expression in cortex, hippocampus and thalamus (areas recorded from experiments described in Figures 1-2). *B-D*, High magnification confocal images of areas defined by white rectangles in *A*, showing ChR2-EYFP positive cell bodies (white arrows) and axon fibers in cortex (*B*), CA1 pyramidal layer (*C*) and thalamus (*D*). *E*, Coronal section showing ChR2-EYFP expression in cortex and striatum (areas recorded from experiments described in Figure 3). *F-G*, High magnification images of areas defined by white rectangles in *E*, showing ChR2-EYFP positive cell bodies and axon fibers in cortex (*F*) and striatum (*G*). *H*, Coronal section from a mouse expressing ArchT-GFP in hippocampus. *I-K*, High magnification images corresponding to white rectangles in *H*, showing strong ArchT-GFP expression in neurons in CA1 (*J*), but not in the overlying cortex (*I*) or the subjacent thalamus (*K*).

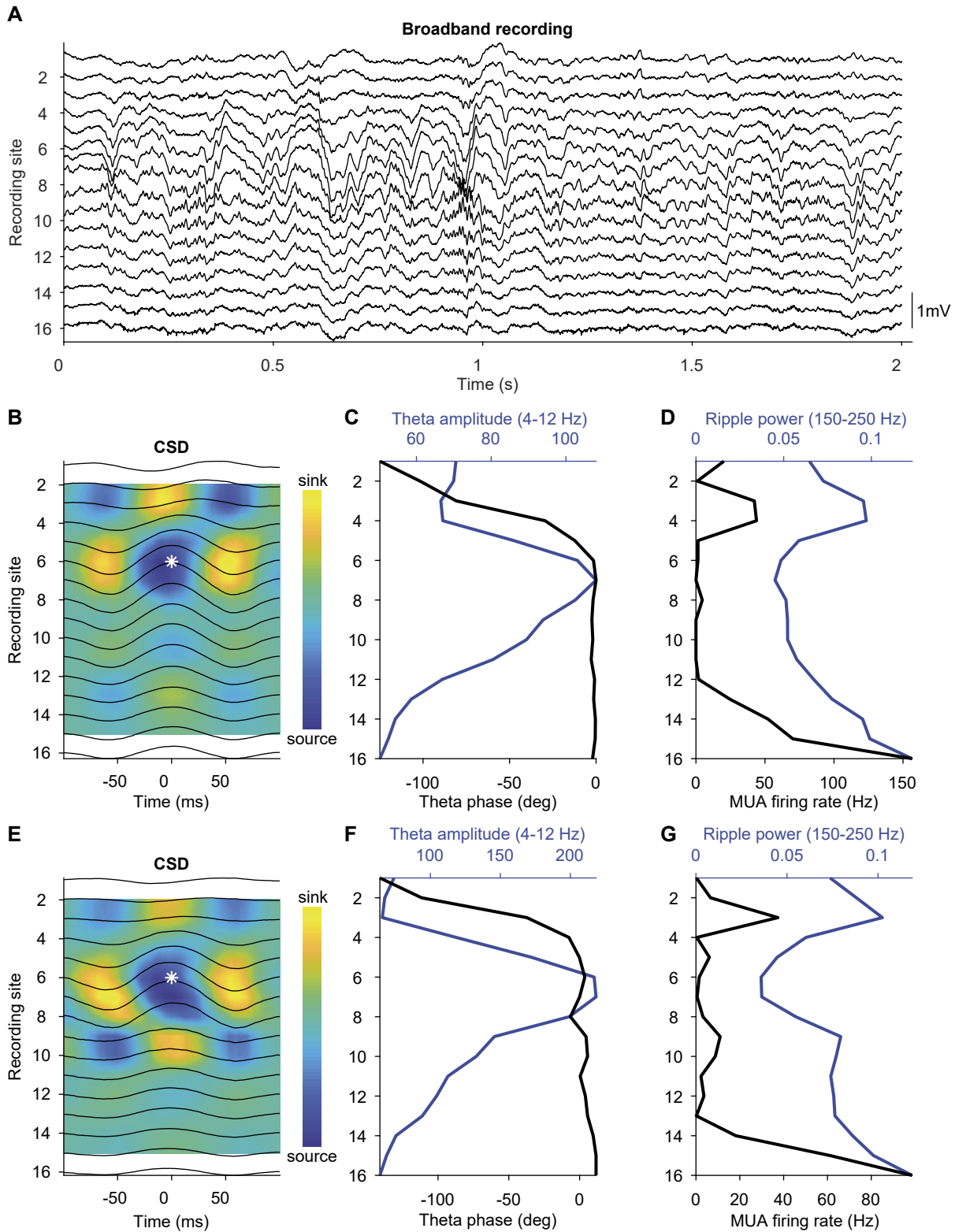


**Figure S2, Signatures of hippocampal activity used for identifying recording positions, related to Figures 1, 2, 6 and STAR Methods.** *A*, Example broadband recording from a 16-channel optoprobe with recording sites in hippocampus and thalamus (as in Figure 1C). *B-D*, Hippocampal activity signatures for one example recording. *B*, Averaged peak-triggered theta (4-12 Hz) oscillations (black traces) and the corresponding CSD (color plot). White asterisk indicates a current source in the hippocampal fissure. *C*, Theta phase (black) and theta amplitude (blue) across recording sites reveals the largest amplitude on channel 7 indicating the location of the hippocampal fissure. *D*, Ripple power (blue) and mean multi-unit firing rate (black) across recording channels. A local maximum can be observed at channels 3-4, indicating the pyramidal layer. *E-G*, Same as in *B-D* but for another example recording.

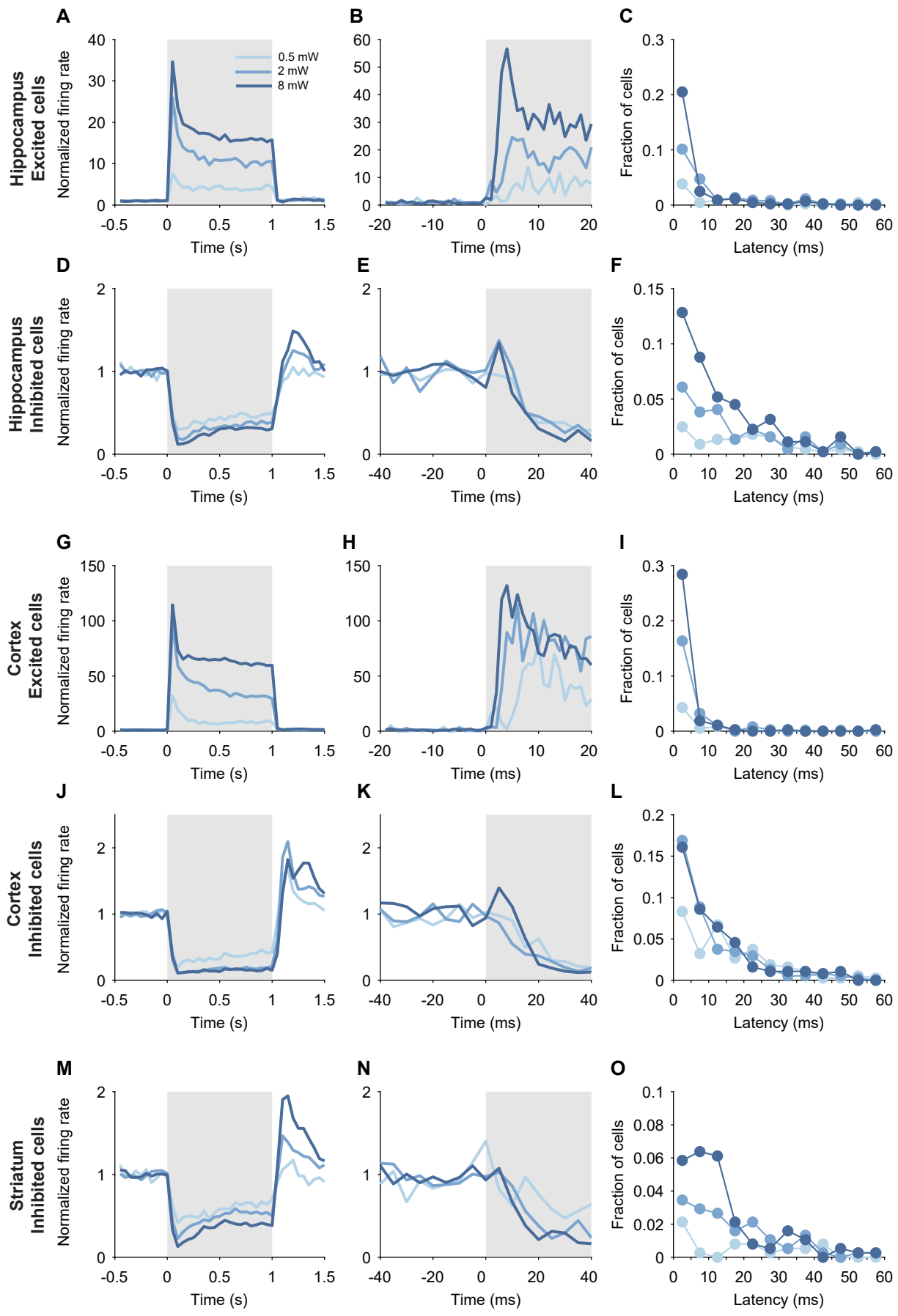


**Figure S3, Time course and latency of excitatory and inhibitory responses in VGAT-ChR2 mice, related to Figures 1-4.** *A*, Average normalized firing rates of significantly excited cells recorded in the hippocampus during light stimulation at different intensities (bin size: 50 ms). *B*, Same as in *A* but with a finer temporal resolution (bin size: 1 ms) to show the response at light onset. *C*, Distribution of response latencies (see STAR Methods) of excited hippocampal neurons for different light intensities. Tick marks on the x-axis represent the edges of 5-ms bins. Most neurons responded at a short latency of < 5 ms. *D-F*, Same as in *A-C* but for hippocampal neurons that were significantly inhibited (bin size in *E*: 5 ms). *G-L*, Time course and latency distribution of excited (*G-I*) and inhibited (*J-L*) neurons in the parietal and somatosensory cortex, shown as in *A-F*. *M-O*, Mean normalized firing rate (*M, N*) and latency distribution (*O*) of significantly inhibited cells recorded in striatum during light stimulation at different intensities.

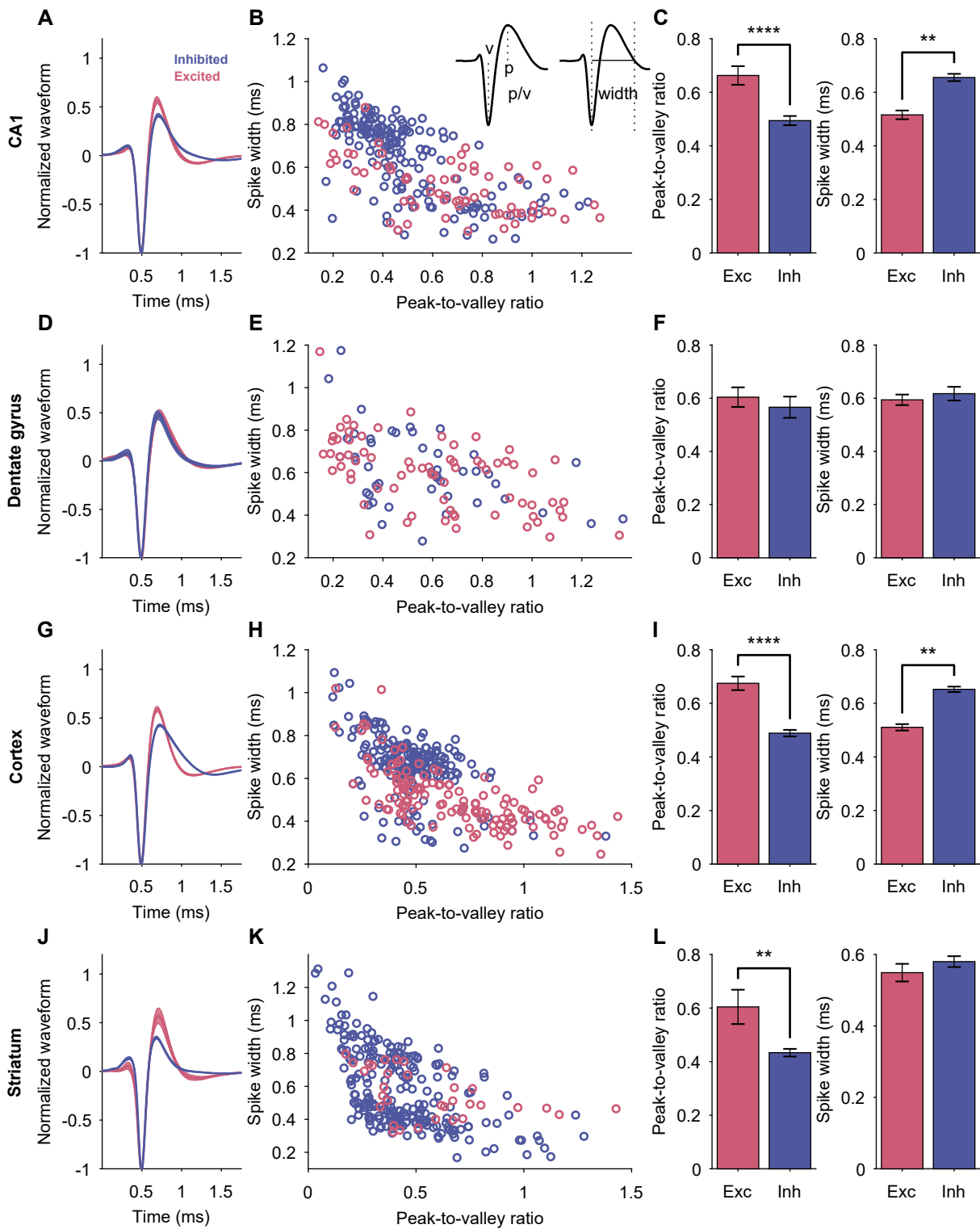


**Figure S4, Action potential waveforms of excited and inhibited neurons in VGAT-ChR2 mice, related to Figures 1-4.** *A*, Normalized waveforms of excited and inhibited cells recorded in the CA1 region of the hippocampus. *B*, Scatter plot of peak-to-valley ratio against spike width (see example waveforms in inset) of significantly excited and inhibited cells in CA1. *C*, Comparison of peak-to-valley ratio (left) and spike width (right) reveals that waveforms of excited CA1 neurons are narrower and have a larger peak-to-valley ratio, suggesting that they are inhibitory interneurons. *D-L*, Waveform analyses as in *A-C* of cells recorded in dentate gyrus (*D-F*), somatosensory and parietal cortex (*G-I*) and striatum (*J-L*). Error bars and shaded areas represent the mean  $\pm$  s.e.m. over neurons. \*\* $p < 0.01$ ; \*\*\*\* $p < 0.0001$

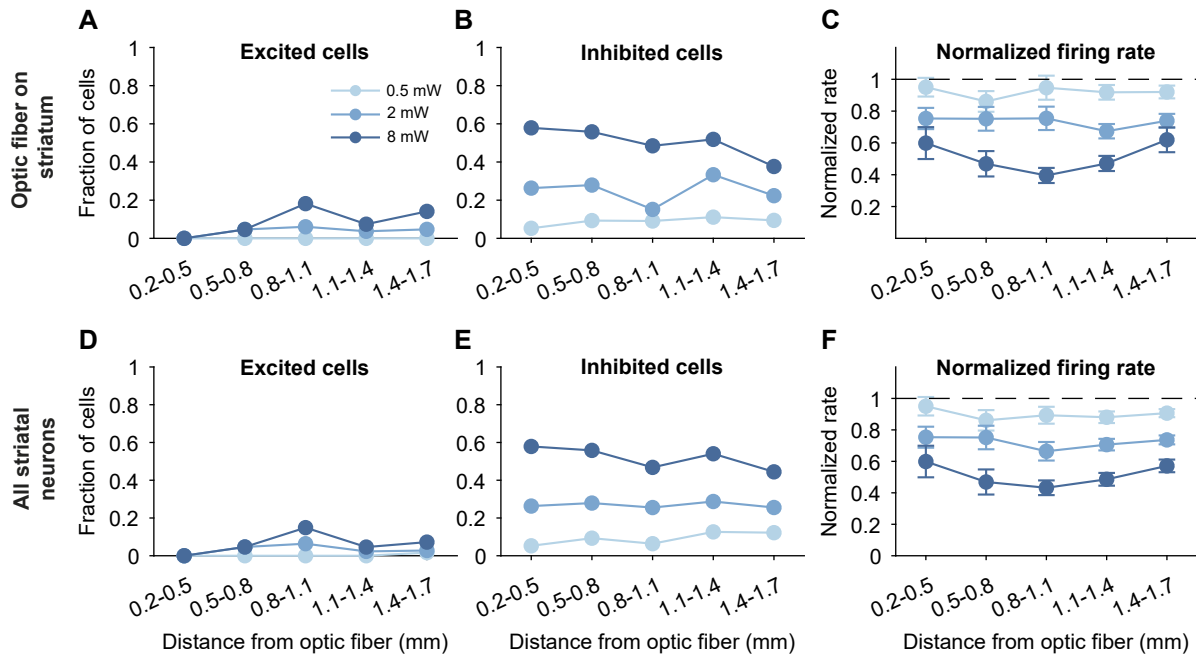


**Figure S5, Excitation and inhibition in striatal cells from VGAT-ChR2 mice, related to Figure 3. A-C,** Fraction of significantly excited (A) and inhibited (B) cells and normalized firing rates (C) of cells recorded in the striatum with the optic fiber on the optoprobe located on top of the striatum (n=234 cells from 3 mice). **D-F,** same as for A-C but for all recorded striatal neurons combined, including those shown in Figure 3 (n=376). Error bars and shaded areas represent the mean  $\pm$  s.e.m. over neurons.

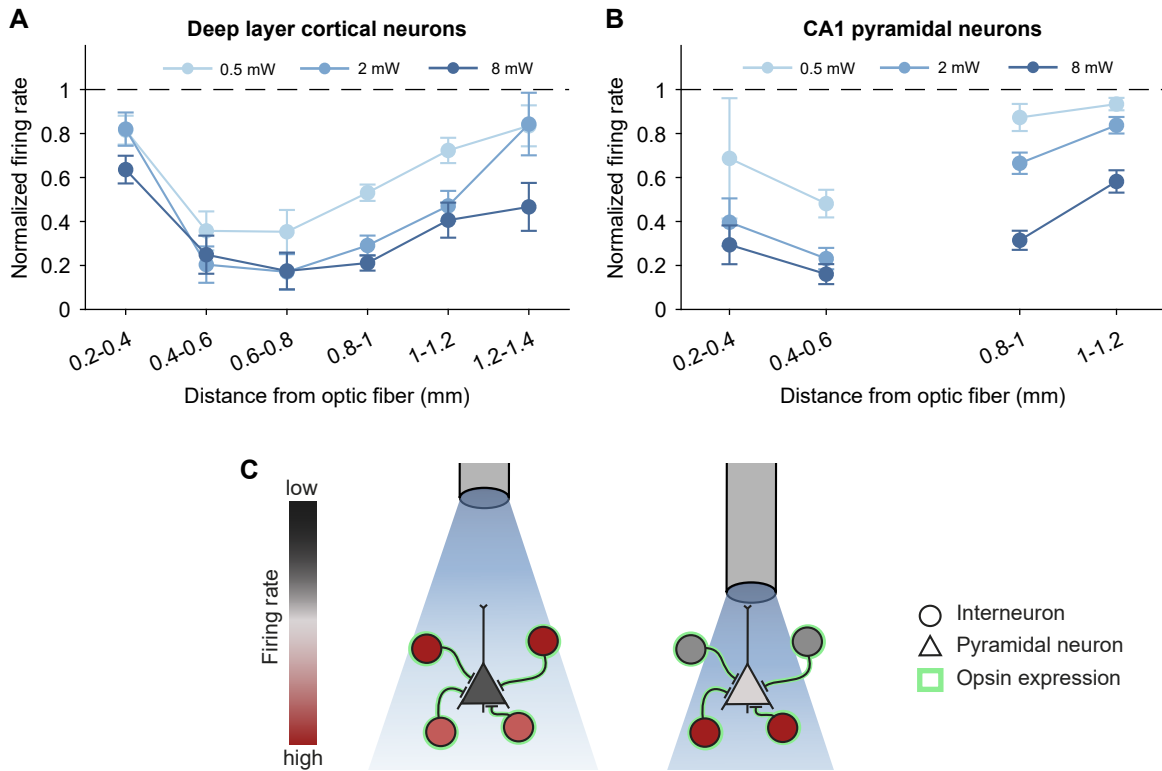


**Figure S6, Inhibition in specific neuronal populations in VGAT-ChR2 mice as a function of distance from the optic fiber, related to Figure 4.** *A*, Normalized firing rates of putative excitatory cells recorded in deep layers of the parietal cortex ( $\geq 500 \mu\text{m}$  below brain surface) and the somatosensory cortex ( $\geq 700 \mu\text{m}$  below brain surface) as a function of distance from the optic fiber. *B*, Normalized firing rate of putative pyramidal cells recorded in the pyramidal layer ( $\pm 100 \mu\text{m}$ ) of CA1, as a function of distance from optic fiber. For both neuronal populations, inhibition was weaker right below the fiber compared to slightly further away (1st vs 2nd distance bin; main effect of distance in a distance X intensity ANOVA:  $p < 0.0001$  for both deep layer cortical neurons and CA1 pyramidal layer neurons). Error bars represent the mean  $\pm$  s.e.m. over neurons. *C*, Schematic explanation for why inhibition is weaker closer to the optic fiber. Because of the horizontal spread of light in brain tissue, a larger proportion of a neuron's inhibitory input population is recruited when the optic fiber is further away.

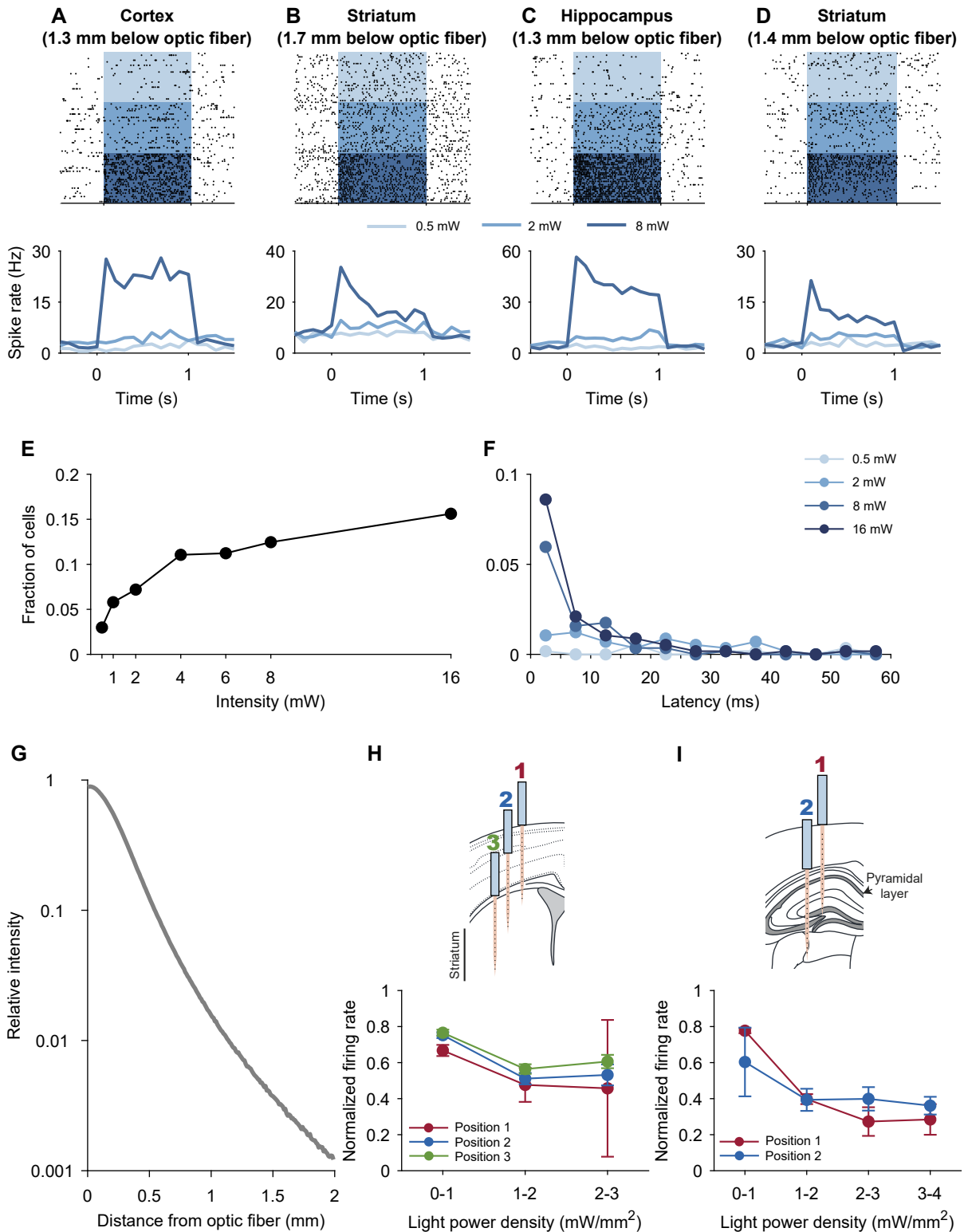


**Figure S7, Optogenetic activation of interneurons far from the optic fiber and comparison of neuronal silencing at different optic fiber positions in VGAT-ChR2 mice, related to Figures 4 and 5.** *A-D*, Examples of neurons in cortex (*A*), striatum (*B, D*) and hippocampus (*C*) that were recorded 1.3-1.7 mm from the optic fiber (distance is specified in heading). *E-F*, Fraction of excited cells recorded  $\geq 1.2$  mm from the optic fiber (*E*) and their response latency distribution (*F*). Tick marks on the x-axis of *F* represents the edges of 5-ms bins. *G*, Estimated relative light intensity as a function of distance from the optic fiber (based on Stujenske et al., 2015; see STAR Methods). *H*, Top, Inhibition in striatal neurons was compared when the optic fiber was above the cortex (Position 1), 0.5 mm below the cortical surface (Position 2) and above the striatum (Position 3). Bottom, Normalized firing rates as a function of light intensity when the optic fiber was in each of the three positions. *I*, Top, Inhibition in CA1 pyramidal neurons was compared when the optic fiber was above the cortex (Position 1) or above the hippocampus (Position 2). Bottom, Normalized firing rates of CA1 pyramidal neurons as a function of light intensity when the optic fiber was in one of the two positions. Error bars represent the mean  $\pm$  s.e.m. over neurons.

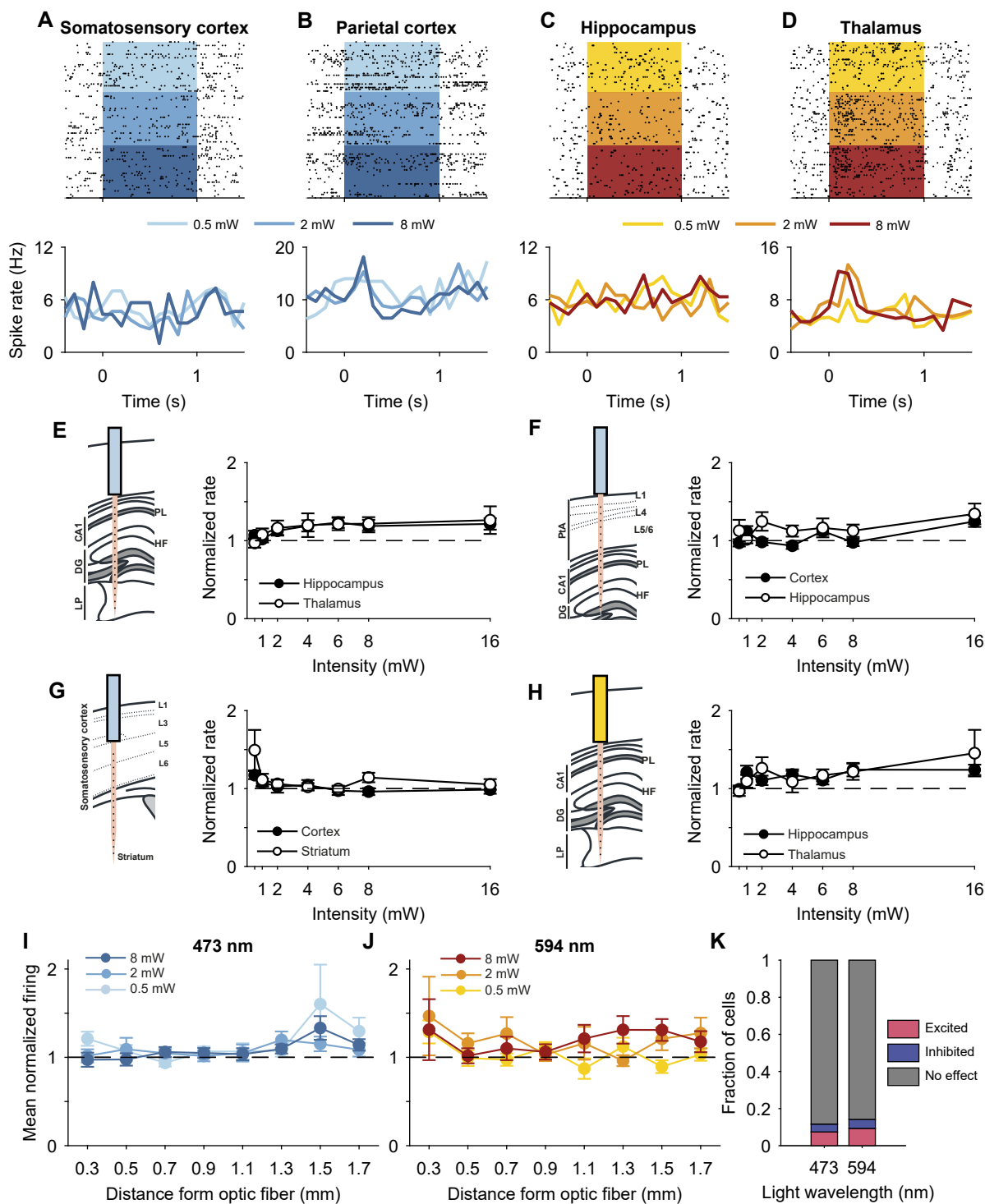


**Figure S8, Effect of light on neuronal activity in mice without opsin expression, related to Figures 1-3 and 6.** *A-D*, Responses of neurons in the somatosensory cortex (*A*), parietal cortex (*B*), hippocampus (*C*) and thalamus (*D*) to blue (*A-B*) and yellow (*C-D*) light in opsin-free mice. Neurons in *A-C* were recorded close ( $\leq 0.5$  mm) to the optic fiber. A few neurons showed transient excitatory responses (*B*, *D*). *E-G*, Normalized firing rates during blue light delivery to different brain regions: hippocampus and thalamus (*E*, compare with Figure 1), cortex and hippocampus (*F*, compare with Figure 2) and cortex and striatum (*G*, compare with Figure 3). *H*, Normalized firing rates in hippocampus and thalamus during yellow light delivery (compare with Figure 6). *I-J*, Normalized firing rates as a function of distance from the optic fiber for blue (*I*) and yellow (*J*) light stimulation. *K*, Fraction of cells that were significantly excited by light stimulation at each wavelength. Error bars represent the mean  $\pm$  s.e.m. over neurons.